Contents

1

Introduction

Modern microfabrication techniques enable one to make very small superconducting mesoscopic structures. Mesoscopic structures here are those which have dimensions of the order of the coherence length ξ or the magnetic penetration depth λ. Because of the small sizes their superconducting properties can be quite different from those of macroscopic samples.

Recently, many mesoscopic superconducting samples have been studied experimentally and theoretically, for example, thin disk (Refs. [1][2][3][4][5][6][7]), mesoscopic cylinder (Refs. [8][9]), mesoscopic ring (Refs. [3][10]), mesoscopic sphere (Ref. [11][12]) and so on. The Ginzburg-Landau (GL) theory is the appropriate framework to study such small superconductors. One distinguishes approaches based on (i) the nonlinear GL equations which is valid away from the superconducting/normal state boundary; and (ii) the linearized GL (LGL) equation which is valid near that boundary.

In this thesis, we study a superconducting mesoscopic circular cone surrounded by vacuum. This is a model for a superconducting STM (scanning tunnel microscopy) tip (see Fig. 1.1). The latter has been used to investigate the properties of superconducting surfaces (Ref. [14]). The superconducting states near the superconducting/normal state boundary are investigated which we extend further into the superconducting region. Within the limited time frame, we consider the approximation in which the superconducting wavefunction can be approximated by a linear combination of solutions of the LGL equation. The LGL equation has been used successfully to describe small mesoscopic samples in the whole magnetic field-temperature (H-T) region (see Ref. [1]).

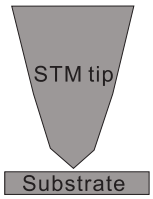

Fig. 1.1 A illustration of a scanning tunneling microscope tip (Ref. [13]).

We make use of the software packages COMSOL (which is based on the finite element method) and MATLAB to obtain the relations of the LGL equation for a cone geometry from which we calculate the Gibbs free energy. We find the vortex configurations and the Cooper-pair density distribution for different vortex states and the ground state mixed by the giant vortex state and multivortex states.

Chapter 1 gives a short introduction of the history of superconductivity. The Ginzburg-Landau theory is discussed. We also introduce the linearized Ginzburg-Landau equation which is the basis of our work.

Chapter 2 gives the expressions for the Gibbs free energy and the order parameter which are obtained from the LGL equation for superconducting mesoscopic circular cones surrounded by vacuum. The cases for giant vortex states and multivortex states are discussed separately. Moreover, the stability conditions for each kind of superconducting state are shown in this chapter. The vorticity of giant vortex states and multivortex states is also introduced at the end of this chapter.

Chapter 3 shows the theoretical results for the giant vortex states in a superconducting mesoscopic circular cone. We show the largest vorticity distribution of giant vortex states for different heights and opening angles of circular cones. We obtaine the eigenvalue, the order parameter and the free energy of the giant vortex states for different vorticities and sizes of the circular cone.

Chapter 4 shows the theoretical results for the multivortex states. The Gibbs free energy, the Cooper-pair density, the phase of the order parameter, the ground state and the vortex configuration are investigated for different sizes of circular cones at different magnetic fields.

Chapter 5 gives the conclusion, in which we will summarize the most important results of this thesis.

1.1 HISTORICAL SURVEY OF SUPERCONDUCTIVITY

In 1911, superconductivity was first observed in mercury by the Dutch physicist Heike Kamerkingh Onnes. When he cooled mercury to the temperature of liquid helium, its resistance suddenly disappeared. This phenomenon was

the so-called *superconductivity*. Two years later, he won the Nobel Prize in physics. In 1933, the German researchers Walter Meissner and Robert Ochsenfeld discovered the second basic electromagnetic property that a superconducting material will repel the magnetic field. This phenomenon is known as the *Meissner effect*.

In 1935, the brothers F. and H. London proposed two equations which can phenomenologically explain these basic electrodynamic properties. This first phenomenological theory proved to be valid in describing the vortex states in extreme type-II superconductors. But it treats vortices as points and does not consider the finite size and the inner structure of the vortex.

In 1950, Ginzburg and Landau developed another well-known phenomenological theory, the so-called *Ginzburg-Landau theory*. It introduces a complex pseudo wave function as an order parameter for the superconducting electrons such that the local density of superconducting electrons is the square of the absolute value of this order parameter. When first proposed, the theory appeared rather phenomenological, and its importance was not generally appreciated.

In 1957, American physicists John Bardeen, Leon Cooper, and John Schrieffer produced the first widely-accepted theory for superconductivity (*BCS theory*). And they won the Nobel Prize for it in 1972. The mathematically-complex BCS theory explained superconductivity at temperatures close to absolute zero for elements and simple alloys. However, for the high temperature superconductors the BCS theory has become inadequate to fully explain superconductivity in these new materials.

In 1957, Abrikosov found a method to classify the superconductors according to the value of the parameter κ in the GL theory. He also predicted the vortex array in the mixed state between H_{c1} and H_{c2}. In 2003, both Abrikosov and Ginzburg won the Nobel Prize in physics for this theory.

In 1959, Gor'kov proved that the GL theory was in fact a limiting form of the microscopic theory of BCS theory, valid near T_c, in which the order parameter can be considered as the wavefunction of the center-of-mass motion of the Cooper-Pair.

In 1962, Brian D. Josephson predicted that electrical current would flow between two superconducting materials, even when they are separated by an insulator. This tunneling phenomenon is known as the Josephson Effect. He won a share of the 1973 Nobel Prize in physics.

In 1986, Alex Müller and Georg Bednorz discovered the first high-T_c superconductor with T_c of 38K. Subsequently many kinds of cuprates have been found with increasing critical temperature. They obtained the 1987 Nobel Prize in physics.

Up to now, the development of theory does not keep up with the new experiment discoveries. The electron-phonon mechanism became questionable. The classic BCS theory was unable to account for many of the properties of high-T_c materials.

1.2 THE GINZBURG-LANDAU THEORY

1.2.1 The Order Parameter and Gibbs Free Energy

In this section, we will present the Gizurg-Landau theory. First, Gizurg and Landau introduced the wave function for superconducting electrons $\Psi(\vec{r})$ as a complex order parameter which is nonzero for $T < T_c$ and vanishes for $T \geq T_c$. Based on the theory of second-order phase transitions developed by Landau, they chose the normalization of this wave function such that $|\Psi(\vec{r})|^2$ gives the density of Cooper-pairs:

$$|\Psi(\vec{r})|^2 = n_s/2, \tag{1.1}$$

where n_s is the density of the superconducting electrons.

The Gibbs free energy density closed to the critical temperature T_c can be expanded as Ref. [15]

$$\mathcal{F}_s = \mathcal{F}_n + \alpha |\Psi|^2 + \frac{\beta}{2} |\Psi|^4 + \frac{1}{2m^*} \left| \left(-i\hbar\vec{\nabla} - \frac{2e}{c}\vec{A} \right) \Psi \right|^2 - \int_0^{H_a} \vec{M} \cdot d\vec{H}_a, \tag{1.2}$$

with the phenomenological constants $\alpha(< 0)$, $\beta(> 0)$, and m^*(the mass of one Cooper-pair). When the state is very close to the superconducting/normal transition at the critical temperature T_c, the expansion of the free energy in powers of the order parameter is a good approximation. The GL theory is valid when temperature is sufficiently near T_c and the spatial variations of Ψ and $\vec{A}$ are not too rapid. But it seems that this theory is used successfully to describe mesoscopic samples in the whole H-T region (see Ref. [16]).

- $\mathcal{F}_n$ is the free energy density of the normal state.
- $\alpha |\Psi|^2 + \frac{\beta}{2} |\Psi|^4$ is a typical Landau form for the expansion of the free energy in terms of an order parameter that vanishes at a second-order phase transition. This term may be viewed as $\alpha n_s + (\beta/2) n_s^2$ and by itself is a minimum with respect to n_s when $n_s = \alpha/\beta$.
- The term $\frac{1}{2m^*} \left| \left(-i\hbar\vec{\nabla} - \frac{2e}{c}\vec{A} \right) \Psi \right|^2$ represents an increase in energy caused by a spatial variation of the order parameter. It has the form of the kinetic energy in quantum mechanics. Here the charge is $2e$, and the mass m^* is $2m_e$ for an electron pair.
- The last term $-\int \vec{M} \cdot d\vec{H}_a$ with the magnetization $\vec{M} = (\vec{H} - \vec{H}_a)/4\pi$, represents the increase in the superconducting free energy caused by the expulsion of magnetic flux from the superconductor. This term can also be written as $-\frac{\vec{h} - \vec{H}}{4\pi} \cdot \vec{H}$, where h is the local magnetic field at a given point of the superconductor and H is the external applied magnetic field.

The overall Gibbs free energy of a superconductor is

$$F_{sH} = F_{nH} + \int \Big\{ \alpha \left|\Psi\right|^2 + \frac{1}{2}\beta \left|\Psi\right|^4 + \frac{1}{2m^*} \left| \Big(-i\hbar\vec{\nabla} - \frac{2e}{c}\vec{A} \Big)\Psi \right|^2 - \frac{\vec{H}' - \vec{H}}{4\pi} \cdot \vec{H} \Big\} dV, \tag{1.3}$$

where the integration is carried out over the entire space V. By minimizing F_{sH} with respect to $\Psi(\vec{r})$ and $\vec{A}(\vec{r})$ we will get the Ginzburg-Landau equations.

1.2.2 The Ginzburg-Landau Equations

The well-known Ginzburg-Landau equations are

$$\alpha\Psi + \beta \left|\Psi\right|^2 \Psi + \frac{1}{2m^*} \Big(-i\hbar\vec{\nabla} - \frac{2e}{c}\vec{A} \Big)^2 \Psi = 0, \tag{1.4}$$

$$\vec{j}_S = -\frac{i\hbar e}{m^*} \big(\Psi^* \vec{\nabla}\Psi - \Psi\vec{\nabla}\Psi^* \big) - \frac{4e^2}{m^* c} \left|\Psi\right|^2 \vec{A}, \tag{1.5}$$

where the current density $\vec{j}_S = \frac{c}{4\pi}\nabla \times \nabla \times \vec{A}$, with the boundary condition

$$\vec{n} \cdot \Big(-i\hbar\vec{\nabla} - \frac{2e}{c}\vec{A} \Big)\Psi \Big|_{boundary} = 0. \tag{1.6}$$

To obtain the first Ginzburg-Landau equation, we should minimize $\mathcal{F}_{sH}$ with respect to $\Psi(\vec{r})^*$ [15]:

$$\int \Big\{ \alpha\Psi\delta\Psi^* + \beta\Psi \left|\Psi\right|^2 \delta\Psi^* + \frac{1}{2m^*}\vec{\varphi} \cdot \Big(i\hbar\vec{\nabla} - \frac{2e}{c}\vec{A} \Big)\delta\Psi^* \} dV = 0, \tag{1.7}$$

where

$$\vec{\varphi} = \Big(-i\hbar\vec{\nabla} - \frac{2e}{c}\vec{A} \Big)\Psi, \tag{1.8}$$

and V is the volume of the superconducting sample. The integration is restricted to the sample because outside this region Ψ is equal to zero.

By making use of the following relations

$$\vec{\nabla} \cdot (\psi\vec{a}) = \vec{a} \cdot \vec{\nabla}\psi + \psi\vec{\nabla} \cdot \vec{a}, \tag{1.9}$$

$$Gauss\ \ theorem: \int \vec{\nabla} \cdot \vec{a} dV = \oint d\vec{S} \cdot \vec{a}, \tag{1.10}$$

$$London\ \ gauge: \vec{\nabla} \cdot \vec{A} = 0, \tag{1.11}$$

where ψ is a scalar quantity, $\vec{a}$ is a vector, $\vec{A}$ is a vector potential and $\vec{n}$ is the unit vector normal to the surface of the sample, one can easily get the first

GL equation (Eq. (1.4)) and the boundary condition (Eq. (1.6)) on the basis of Eq. (1.7).

To obtain the second Ginzburg-Landau equation, we should minimize $\mathcal{F}_{sH}$ with respect to $\vec{A}$ [15]:

$$\begin{aligned}\frac{1}{2m^*}\int\Bigg[&\Big(-\frac{2e}{c}\delta\vec{A}\Psi^*\Big)\cdot\Big(-i\hbar\vec{\nabla}\Psi-\frac{2e}{c}\vec{A}\Psi\Big)\\&+\Big(-\frac{2e}{c}\delta\vec{A}\Psi\Big)\cdot\Big(i\hbar\vec{\nabla}\Psi^*-\frac{2e}{c}\vec{A}\Psi^*\Big)\Bigg]dV\\&+\frac{1}{4\pi}\int\left(\nabla\times\vec{A}-\vec{H}\right)\cdot\nabla\times\delta\vec{A}dV=0,\end{aligned}\tag{1.12}$$

with $\vec{H}=\nabla\times\vec{A}$, and V the volume of the entire space.

By making use of Gauss theorem and the following relation

$$\vec{\nabla}\cdot(\vec{a}\times\vec{b})=\vec{b}\cdot\vec{\nabla}\times\vec{a}-\vec{a}\cdot\vec{\nabla}\times\vec{b},\tag{1.13}$$

the second GL equation (Eq. (1.5)) can also be derived easily.

1.2.3 Further Discussion

Here we discuss three important parameters in the Ginzburg-Landau theory: the coherence length $\xi(T)$, the penetration depth $\lambda(T)$ and the Ginzburg-Landau parameter κ.

Coherence Length $\xi(T)$. Coherence length $\xi(T)$ is the characteristic length for variation of Ψ (see Ref. [17])

$$\xi^2(T)=\frac{\hbar^2}{2m^*|\alpha(T)|}.\tag{1.14}$$

It can be easily understood if there is no magnetic field present. By introducing $f=\Psi/(\Psi_0)$ where $\Psi_0=\sqrt{-\alpha/\beta}$ and f is a real function because of $\vec{A}=0$, the first GL equation can be written as

$$\xi^2(T)\frac{d^2f}{dx^2}+f+f^3=0.\tag{1.15}$$

Moreover, using $g=f-1$ instead of f and expanding the above equation with respect to g, we will have

$$\xi^2(T)\frac{d^2g}{dx^2}=2g,\tag{1.16}$$

and the solution of this equation

$$g(x)\sim e^{\pm\sqrt{2}x/\xi(T)}.\tag{1.17}$$

This shows that a small disturbance of Ψ from Ψ_0 will decay over a characteristic length of order $\xi(T)$.

Since α depends on temperature as $|\alpha| \propto \left(T_{c0} - T\right)$ (where T_{c0} is the critical temperature without magnetic field), the coherence length ξ varies as function of temperature as

$$\xi(T) \propto \left(T_{c0} - T\right)^{-1/2}. \tag{1.18}$$

Penetration Depth λ. Penetration depth $\lambda(T)$ is the characteristic length for variation of magnetic field: (see Ref. [18])

$$\lambda^2(T) = \frac{m^* c^2}{16\pi e^2 \left|\Psi_0\right|^2}. \tag{1.19}$$

Let us consider the simple situation that inside the superconducting sample $\Psi = \Psi_0$ and take the *curl* of both sides of the second GL equation (Eq. (1.5)):

$$rot\, \vec{j}_S = -\frac{4e^2}{m^* c} \left|\Psi\right|^2 \nabla \times \vec{A} \tag{1.20}$$

Using the Maxwell equation $\nabla \times \vec{j}_S = \nabla \times \nabla \times \vec{H}$, $\nabla \times \vec{A} = \vec{H}$ and the definition of $\lambda(T)$ we can rewrite this as

$$\vec{h} + \lambda^2(T) \nabla \times \nabla \times \vec{h} = 0. \tag{1.21}$$

This shows that the magnetic field will decay over a characteristic length of order $\lambda(T)$.

The penetration depth $\lambda(T)$ also varies as function of temperature as

$$\lambda(T) \propto \left(1 - T/T_{c0}\right)^{-1/2}, \tag{1.22}$$

since $\left|\Psi_0\right|^2 \propto |\alpha| \propto \left(T_{c0} - T\right)$ while β is a constant near T_c.

The Ginzburg-Landau Parameter κ. Superconductors can be separated into two types according to the values of their Ginzburg-Landau parameter $\kappa = \frac{\lambda(T)}{\xi(T)}$ (Refs. [18] and [19]):

$$\kappa < 1/\sqrt{2} \rightarrow \mathit{Type\ I\ superconductors}, \tag{1.23}$$

$$\kappa > 1/\sqrt{2} \rightarrow \mathit{Type\ II\ superconductors}. \tag{1.24}$$

It is found that except Niobium, all simple metals are type-I superconductors. Niobium and all superconducting alloys and chemical compounds are type-II. The new found high-T_c superconductors are also type-II superconductors.

For $\kappa < 0.42$ at a magnetic field below thermodynamical critical field H_c the superconductor is in the Meissner state and all flux is expelled from the sample. At the critical field the magnetic field penetrates the sample, superconductivity is destroyed and the sample becomes normal.

For $0.42 < \kappa < 0.71$ the superconductor is still a type-I superconductor. At the field H_c flux can penetrate the inner part of the sample, while the surface of the sample remains superconducting. At the surface critical field H_{c3} the whole sample will be normal.(Refs. [15][20][21])

In type-II superconductors ($\kappa > 0.71$), the Meissner state appears only at an applied field below the first critical field H_{c1}. In the region between H_{c1} and the second critical field H_{c2} the magnetic flux is able to penetrate the sample in quantized units of the flux quantum $\phi_0 = hc/2e$. This state is called the Mixed state. In the region $H_{c2} < H < H_{c3}$, superconductivity only exists at the surface of the sample, while the inner part is in the normal state. For bulk type-II superconductors the third critical field H_{c3} is approximately equal to $1.7H_{c2}$. For larger fields the entire sample is in the normal state. (Refs. [17] and [21])

1.3 LINEARIZED GINZBURG-LANDAU EQUATION

Linearized Ginzburg-Landau (LGL) equation is obtained by ignoring the second term on the left side of Eq. (1.4). This equation is often applied to study the superconducting properties of mesoscopic samples at the superconducting/normal state boundary. The Cooper-pair density is very small and the demagnetization effects are neglected, i.e. the magnetic field equals the external one. A number of works studied disk and ring geometries (Refs. [1][2][3][4][5][6][22]) in the framework of the LGL equation where a uniform magnetic field is assumed. Transport measurements in individual mesoscopic disks supported the theoretic results quite well, such as the oscillations of critical temperature as a function of the external magnetic field could be explained by solving the LGL equation (Ref. [23]).

Suppose that now we have a mesoscopic sample in a uniform magnetic field, and want to study its properties near the superconducting/normal boundary. Then it will be quite suitable to solve the LGL equation .

The linearized Ginzburg-Landau equation is:

$$\frac{1}{2m^*}\left(-i\hbar\vec{\nabla} - \frac{2e}{c}\vec{A}\right)^2\Psi + \alpha\Psi = 0. \tag{1.25}$$

With $\nabla \cdot \vec{A} = 0$, we can write it in another form:

$$\nabla^2\Psi - \frac{4ie}{\hbar c}\vec{A}\cdot\nabla\Psi - \frac{4e^2}{\hbar^2c^2}\vec{A}^2\Psi = \frac{2m^*\alpha}{\hbar^2}\Psi. \tag{1.26}$$

Then, by expressing the distance in units of the coherence length $\xi(T)$, the vector potential $\vec{A}$ in $c\hbar/2e\xi(T)$ and the order parameter in $\Psi_0 = \sqrt{|\alpha|/\beta}$, we have

$$\nabla^2\Psi - 2i\vec{A}\cdot\nabla\Psi - \vec{A}^2\Psi = \frac{2m^*\alpha\xi^2(T)}{\hbar^2}\Psi. \tag{1.27}$$

With Eq. (1.14), the dimensionless linearized GL equation can be rewritten as

$$\nabla^2\Psi - 2i\vec{A}\cdot\nabla\Psi - \vec{A}^2\Psi = -\Psi. \tag{1.28}$$

We restrict ourselves to a sufficiently small sample such that the size is much smaller than the penetrating length λ and comparable to the coherence length ξ, so we let $h \approx H$ and neglect the last term in the free energy expression (Eq. (1.3)). This approximation is valid for extreme type-II superconductors, for very small superconductors and near the superconducting/normal phase boundary. Using dimensionless units the total Gibbs free energy of the superconducting states, measured in $F_0 = \alpha^2/2\beta$, is determined by the expression

$$F = 2\bigg[\int dV\bigg(-|\Psi|^2 + \frac{1}{2}|\Psi|^4 + \Big|-i\vec{\nabla}\Psi - \vec{A}\Psi\Big|^2\bigg)\bigg], \tag{1.29}$$

where we set the normal part of the free energy $F_n = 0$ and V is the volume of the sample measured in $\xi^3(T)$. The best choice for normalization of the free energy is $F_0 = \alpha^2/2\beta = \frac{H_c^2}{8\pi}$. The quantum $\frac{H_c^2}{8\pi}$ is the energy of the condensate in general

$$F_{normal} - F_{superconducting} = \frac{H_c^2}{8\pi}. \tag{1.30}$$

On the other hand, consider the dimensionless boundary condition

$$\vec{n}\cdot\big(-i\vec{\nabla} - \vec{A}\big)\Psi\Big|_{boundary} = 0, \tag{1.31}$$

and do the integral over the surface of the sample, we will get

$$\begin{aligned}
&\int dS\,\vec{n}\cdot\big(-i\vec{\nabla} - \vec{A}\big)\Psi \\
&\quad= \int dV\,\vec{\nabla}\cdot\bigg(\big(-i\vec{\nabla} - \vec{A}\big)\Psi\bigg) \\
&\quad= \int dV\,\big[-\nabla\Psi\cdot\nabla\Psi^* - \Psi\nabla^2\Psi + i\vec{A}\cdot\big(\Psi\nabla\Psi^* + \Psi^*\nabla\Psi\big)\big] \\
&\quad= 0.
\end{aligned} \tag{1.32}$$

By combining Eq. (1.29) and Eq. (1.32), we can rewrite the Gibbs free energy as

$$\begin{aligned}
F &= 2\bigg[\int dV\bigg(-|\Psi|^2 + \frac{1}{2}|\Psi|^4 + \Psi^*\big(-i\vec{\nabla} - \vec{A}\big)^2\Psi\bigg)\bigg] \\
&= 2\bigg[\int dV\bigg(-|\Psi|^2 + \frac{1}{2}|\Psi|^4 + \Psi^*\big(\nabla^2\Psi - 2i\vec{A}\cdot\nabla\Psi - \vec{A}^2\Psi\big)\bigg)\bigg].
\end{aligned} \tag{1.33}$$

2

Theoretical Formalism

In this chapter we apply the linearized GL equation to a mesoscopic superconductor with the shape of a circular cone surrounded by vacuum with an external uniform magnetic field $\vec{H}$ along the z direction. Because of its small size we can assume that the magnetic field inside the circular cone and outside is equal to $\vec{H}$.

The geometry of our sample is shown in Fig. 2.1. The shape of a circular cone can be described by two parameters: height z_0 and its vertex angle 2θ, or equivalently, the height z_0 and its radius r. The relation between the radius, height and vertex angle is $r = z_0 \times tan(\theta)$. In this thesis, we use the notation (z_0, θ, r) to present the size of a circular cone.

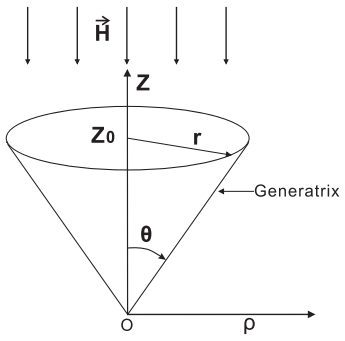

Fig. 2.1 The circular cone.

Circular cones have cylindrical symmetry, so it is advantageous for us to rewrite the dimensionless linearized Ginzburg-Landau equation (Eq. (1.28)) in cylindrical coordinates. According to the form of the external magnetic field ($\vec{H} = H\vec{e_z}$) and the coordinates transformation relations, its vector potential $\vec{A}$ can be rewritten as:

$$\vec{A} = (H\rho/2)\vec{e_\varphi}, \tag{2.1}$$

which satisfies the London gauge $\nabla \cdot \vec{A} = 0$.

Finally, the linearized Ginzburg-Landau equation (Eq. (1.28)) can be rewritten as follows:

$$\frac{1}{\rho}\frac{\partial}{\partial\rho}\left(\rho\frac{\partial\Psi}{\partial\rho}\right) + \frac{1}{\rho^2}\frac{\partial^2\Psi}{\partial\varphi^2} + \frac{\partial^2\Psi}{\partial z^2} - iH\frac{\partial\Psi}{\partial\varphi} - \left(\frac{H\rho}{2}\right)^2\Psi = -\Psi. \tag{2.2}$$

2.1 GIANT VORTEX STATES IN A MESOSCOPIC CIRCULAR CONE

First we consider the giant vortex states, which have cylindrical symmetry because in these states the corresponding Cooper-pair density is independent of the angle φ of cylindrical coordinate system (ρ, φ, z). Their order parameters are of the form:

$$\Psi(\rho, \varphi, z) = C\psi_L(\rho, z)e^{iL\varphi}, \tag{2.3}$$

where the coefficient C is a constant and the angular momentum quantum number L is an integer due to the periodical boundary condition $\Psi(\rho, \varphi, z) = \Psi(\rho, \varphi + 2n\pi, z)$ and n is an integer.

Using Eq. (2.3) and Eq. (2.2), we obtain an equation for $\psi(\rho, z)$:

$$-\frac{\partial^2\psi}{\partial\rho^2} - \frac{\partial^2\psi}{\partial z^2} - \frac{1}{\rho}\frac{\partial\psi}{\partial\rho} + \left(\frac{L^2}{\rho^2} - HL + \frac{H^2\rho^2}{4}\right)\psi = \psi. \tag{2.4}$$

To follow the notation of Refs. [1] and [6] we use the $\hat{L}$ operator (but the definition is different), given by

$$\hat{L} = -\frac{\partial^2}{\partial\rho^2} - \frac{\partial^2}{\partial z^2} - \frac{1}{\rho}\frac{\partial}{\partial\rho} + \left(\frac{L^2}{\rho^2} - HL + \frac{H^2\rho^2}{4}\right) - 1, \tag{2.5}$$

and Eq. (2.4) will become

$$\hat{L}\psi_{L,n}(\rho, z) = 0, \tag{2.6}$$

where $n(= 0, 1, 2, 3...)$ enumerates the different states at a certain angular momentum quantum number L.

The dimensionless nonlinear first GL equation is

$$\hat{L}\psi_{L,n}(\rho, z) = -|\Psi|^2\psi_{L,n}, \tag{2.7}$$

so, the superconducting states should correspond to the negative eigenvalues of the $\hat{L}$ operator when we use the linearized GL equation to simulate the nonlinear first GL equation.

We should solve the equation

$$\boxed{\hat{L}\psi_{L,n}(\rho,z)=\Lambda_{L,n}\psi_{L,n}(\rho,z).} \tag{2.8}$$

Here in our work we restrict ourself to $n=0$. From now on, we drop the n in $\psi_{L,n}$ in favor of a short notation for the giant vortex states. If there is no extra note, then ψ_L stands for $\psi_{L,n=0}$.

The solution $\psi_L(\rho,z)$ for $\hat{L}\psi=\Lambda\psi$ can always be chosen as a real function. If there is a solution ψ_L, then ψ_L^* will also satisfy the same equation $\hat{L}\psi_L^*=\Lambda\psi_L^*$. Because $\hat{L}$ is a linear operator , we can construct a real solution $\psi_L+\psi_L^*$ with the same eigenvalue as for ψ_L.

The Gibbs free energy can be calculated according to Eq. (1.33). Moreover, the constant coefficient C in Eq. (2.3) can be fixed by minimizing the Gibbs free energy.

Substitute the order parameter Ψ (Eq. (2.3)) and the vector potential $\vec{A}$ (Eq. (2.1)) into Eq. (1.33), we can get

$$\begin{aligned}
F &= 2\left[\int dV\left(-|C|^2\psi_L^2+\frac{1}{2}|C|^4\psi_L^4+|C|^2\psi_L(\hat{L}+1)\psi_L\right)\right]\\
&= 2\left[\int dV\left(-|C|^2\psi_L^2+\frac{1}{2}|C|^4\psi_L^4+|C|^2(\Lambda+1)\psi_L^2\right)\right]\\
&= 2\left[\int dV\left(\Lambda|C|^2\psi_L^2+\frac{1}{2}|C|^4\psi_L^4\right)\right]\\
&= 4\pi\Lambda|C|^2 I_2+2\pi|C|^4 I_1,
\end{aligned} \tag{2.9}$$

where

$$I_1=\int_0^{z_0}dz\int_0^{z\times tan(\theta)}\rho d\rho\,\psi_L^4\ \ ,I_2=\int_0^{z_0}dz\int_0^{z\times tan(\theta)}\rho d\rho\,\psi_L^2. \tag{2.10}$$

We can see that whether the coefficient C is real or not does not affect the value of the free energy, so for simplicity we choose C to be *real* and *positive*. Then the Gibbs free energy is a function with one variable C. Now, we minimize the free energy (Eq. (2.9)) with respect to the coefficient C

$$\frac{\partial F}{\partial C}=0, \tag{2.11}$$

with the following condition

$$\frac{\partial^2 F}{\partial C^2}>0, \tag{2.12}$$

we obtain the coefficient C

$$C=\pm\sqrt{-\Lambda\frac{I_2}{I_1}}, \tag{2.13}$$

and the value of the free energy

$$\boxed{F = -2\pi\Lambda^2 \frac{I_2^2}{I_1}.} \tag{2.14}$$

Because of the following equation

$$\frac{\partial^2 F}{\partial C^2} = -16\pi\Lambda I_2, \tag{2.15}$$

we see that any state with a negative eigenvalue is always stable. And the order parameter is

$$\boxed{\Psi(\rho,\varphi,z) = C\psi_L(\rho,z)e^{iL\varphi} = \pm\sqrt{-\Lambda\frac{I_2}{I_1}}\psi_L(\rho,z)e^{iL\varphi}.} \tag{2.16}$$

So, after Eq. (2.8) is solved, the order parameter Ψ, the eigenvalue Λ and the free energy F are easily obtained.

The superconducting current is given by the second Ginzburg-Landau equation (Eq. (1.5)). By measuring the current j_s in unit of $j_0 = 2\hbar e\Psi_0^2/m^*\xi(T)$ and dimensionless operations with respect to the order parameter, vector potential and distance, we have

$$\vec{j_s} = -\frac{1}{2}(\Psi^*\vec{\nabla}\Psi - \Psi\vec{\nabla}\Psi^*) - |\Psi|^2\vec{A}. \tag{2.17}$$

With the equations (Eq. (2.1) and Eq. (2.16)), we can obtain the expression for the superconducting current for the giant vortex state as follows,

$$\vec{j_s} = (\frac{L}{\rho} - \frac{H\rho}{2})C^2\psi_L^2\vec{e_\varphi}, \tag{2.18}$$

where $C^2 = -\Lambda\frac{I_2}{I_1}$.

2.2 MULTIVORTEX STATES IN A MESOSCOPIC CIRCULAR CONE

For a sufficiently large sample the giant vortex can break up into several small vortices which corresponds to a multivortex state (Refs. [4] and [16]). Now we use the linearized Ginzburg-Landau equation as an approximation to the nonlinear equation, so the order parameter of the multivortex states is very suitable to be recognized as a linear combination of the eigenfunctions of the linearized GL equation (Eq. (2.8)) (Refs. [1][2][4]),

$$\Psi(\rho,\varphi,z) = \sum_{L_j=0}^{L}\sum_{n=0}^{\infty} C_{L_j,n}\psi_{L,n}(\rho,z)exp(iL_j\varphi), \tag{2.19}$$

where L is the angular momentum for a certain component, and the numbers $n = 0, 1, 2...$ enumerate the different radial states for the same L.

Following Refs. [1] and [2] we restrict ourselves to the lowest state eigenfunctions and take only $n = 0$. Then the expression of the order parameter can be rewritten as

$$\Psi(\rho, \varphi, z) = \sum_{L_j=0}^{L} C_{L_j} \psi_L(\rho, z) exp(iL_j\varphi). \tag{2.20}$$

By substituting Eq. (2.20) into the Gibbs free energy expression (Eq. (1.33)), we obtain F as a function of the complex parameters $\{C_{L_j}\}$. To obtain the equilibrium vortex configurations and to determine their stability we should minimize F with respect to these parameters.

The following equations are used to determine the values of these parameters $\{C_{L_j}\}$ notated as $\{C^{(0)}_{L_j}\}$ and the stability of the vortex states

$$\frac{\partial F}{\partial C_{Lj}} = 0 \quad and \quad \frac{\partial F}{\partial C^*_{L_j}} = 0, \tag{2.21}$$

$$M_{Hesse} = \begin{pmatrix} \frac{\partial^2 F}{\partial C_0^2}(\{C^{(0)}_{L_j}\}) & \frac{\partial^2 F}{\partial C_0 \partial C_1}(\{C^{(0)}_{L_j}\}) & \cdots & \frac{\partial^2 F}{\partial C_0 \partial C^*_L}(\{C^{(0)}_{L_j}\}) \\ \frac{\partial^2 F}{\partial C_0 \partial C_1}(\{C^{(0)}_{L_j}\}) & \frac{\partial^2 F}{\partial C_1^2}(\{C^{(0)}_{L_j}\}) & \cdots & \frac{\partial^2 F}{\partial C_1 \partial C^*_L}(\{C^{(0)}_{L_j}\}) \\ \cdots & \cdots & \cdots & \cdots \\ \frac{\partial^2 F}{\partial C^*_L \partial C_0}(\{C^{(0)}_{L_j}\}) & \frac{\partial^2 F}{\partial C^*_L \partial C_1}(\{C^{(0)}_{L_j}\}) & \cdots & \frac{\partial^2 F}{\partial C^{*2}_L}(\{C^{(0)}_{L_j}\}) \end{pmatrix}, \tag{2.22}$$

This matrix M_{Hesse} is the so-called **Hessian matrix**. If the state is stable, then its Hessian matrix should be positive definite.

The order parameter of the giant vortex states can also be described by Eq. (2.20) with only one nonzero coefficient $C^{(0)}_{L_j}$. If the corresponding Hessian matrix is positive , the giant vortex state is stable.

Now let us consider the states which are constructed by only two components in Eq. (2.20). Because in this case we can find analytical expressions for the free energy and the order parameter and analytic stability equation for the superconducting states. Substitute the following expression of two-component order parameter Ψ

$$\boxed{\Psi(\rho, \varphi, z) = C_{L_1} \psi_{L_1}(\rho, z) e^{iL_1\varphi} + C_{L_2} \psi_{L_2}(\rho, z) e^{iL_2\varphi}} \tag{2.23}$$

and the vector potential $\vec{A}$ (Eq. (2.1)) into Eq. (1.33), we can obtain the expression for the Gibbs free energy for the two-component state

$$\begin{aligned} F &= 2\Big[\int dV\Big(-|\Psi|^2+\frac{1}{2}|\Psi|^4+\Psi^*(-i\vec{\nabla}-\vec{A})^2\Psi\Big)\Big] \\ &= 2\Big\{\int dV\Big[-\big|C_{L_1}\psi_{L_1}(\rho,z)e^{iL_1\varphi}+C_{L_2}\psi_{L_2}(\rho,z)e^{iL_2\varphi}\big|^2 \\ &\quad +\frac{1}{2}\big|C_{L_1}\psi_{L_1}(\rho,z)e^{iL_1\varphi}+C_{L_2}\psi_{L_2}(\rho,z)e^{iL_2\varphi}\big|^4 \\ &\quad +(C^*_{L_1}\psi_{L_1}(\rho,z)e^{-iL_1\varphi}+C^*_{L_2}\psi_{L_2}(\rho,z)e^{-iL_2\varphi}) \\ &\quad \cdot\big[(\Lambda_{L_1}+1)C_{L_1}\psi_{L_1}(\rho,z)e^{iL_1\varphi}+(\Lambda_{L_2}+1)C_{L_2}\psi_{L_2}(\rho,z)e^{iL_2\varphi}\big]\Big]\Big\} \\ &= 2\pi\big[\,|C_{L_1}|^4 A_{L_1}+|C_{L_2}|^4 A_{L_2}+4\,|C_{L_1}|^2|C_{L_2}|^2 A_{L_1,L_2} \\ &\quad +2\Lambda_{L_1}|C_{L_1}|^2 B_{L_1}+2\Lambda_{L_2}|C_{L_2}|^2 B_{L_2}\big]. \end{aligned} \tag{2.24}$$

At the last step, we use the following relations and definitions

$$\int_0^{2\pi} d\varphi\, e^{i(L_i-L_j)\varphi}=0,\quad L_i\neq L_j\quad and\quad \int_0^{2\pi} d\varphi\, e^{i(L_i-L_j)\varphi}=2\pi,\quad L_i=L_j, \tag{2.25}$$

$$\begin{aligned} A_{L_i} &= \int_0^{z_0} dz\int_0^{z\times tan(\theta)} \rho d\rho\,\psi^4_{L_i}(\rho,z), \\ B_{L_i} &= \int_0^{z_0} dz\int_0^{z\times tan(\theta)} \rho d\rho\,\psi^2_{L_i}(\rho,z), \\ A_{L_1,L_2} &= \int_0^{z_0} dz\int_0^{z\times tan(\theta)} \rho d\rho\,\psi^2_{L_1}(\rho,z)\psi^2_{L_2}(\rho,z). \end{aligned} \tag{2.26}$$

One thing to mention is that if one of the coefficients (C_{L_1}, C_{L_2}) is zero, then this state is a **giant vortex state**; if these coefficients are nonzero, then it is a **multivortex state**; if both of them are zero, then it is a **normal state**.

According to Eq. (2.24), whether C_{L_i} are real or complex does not affect the value of the free energy, so we can regard them as **real**. By minimizing the Gibbs free energy with respect to C_{L_1} and C_{L_2} using Eq. (2.21), we can obtain the possible equilibrium states:

(i) The normal state with $\Psi(\rho,\varphi,z)=0$,

$$C^{(0)}_{L_1}=C^{(0)}_{L_2}=0. \tag{2.27}$$

(ii) The giant vortex states with $\Psi(\rho,\varphi,z)=C^{(0)}_{L_1}\psi_{L_1}e^{iL_1\varphi}$ or $\Psi(\rho,\varphi,z)=C^{(0)}_{L_2}\psi_{L_2}e^{iL_2\varphi}$,

$$\begin{aligned} C^{(0)}_{L_1}=0, &\qquad C^{(0)}_{L_2}=\Big(-\Lambda_{L_2}\frac{B_{L_2}}{A_{L_2}}\Big), \\ or,\quad C^{(0)}_{L_1}=\Big(-\Lambda_{L_1}\frac{B_{L_1}}{A_{L_1}}\Big), &\qquad C^{(0)}_{L_2}=0. \end{aligned} \tag{2.28}$$

(iii) The multivortex states with $\Psi(\rho,\varphi,z)=C_{L_1}^{(0)}\psi_{L_1}e^{iL_1\varphi}+C_{L_2}^{(0)}\psi_{L_2}e^{iL_2\varphi}$, where

$$\begin{aligned} C_{L_1}^{(0)} &= \pm\big(\frac{-\Lambda_{L_1}A_{L_2}B_{L_1}+2\Lambda_{L_2}A_{L_1,L_2}B_{L_2}}{A_{L_1}A_{L_2}-4A_{L_1,L_2}^2}\big)^{1/2}, \\ C_{L_2}^{(0)} &= \pm\big(\frac{-\Lambda_{L_2}A_{L_1}B_{L_2}+2\Lambda_{L_1}A_{L_1,L_2}B_{L_1}}{A_{L_1}A_{L_2}-4A_{L_1,L_2}^2}\big)^{1/2}. \end{aligned} \tag{2.29}$$

Only those coefficients $C_{L_1}^{(0)}$ and $C_{L_2}^{(0)}$ which make the Hessian matrix (Eq. (2.22)) positive definite are physical relevant. This condition can be rewritten as

$$\boxed{\begin{aligned} \frac{\partial^2 F}{\partial C_{L_1}^2}\Big|_{C_{L_1}=C_{L_1}^{(0)},C_{L_2}=C_{L_2}^{(0)}} &> 0, \\ \frac{\partial^2 F}{\partial C_{L_1}^2}\frac{\partial^2 F}{\partial C_{L_2}^2}-(\frac{\partial^2 F}{\partial C_{L_1}\partial C_{L_2}})^2\Big|_{C_{L_1}=C_{L_1}^{(0)},C_{L_2}=C_{L_2}^{(0)}} &> 0, \end{aligned}} \tag{2.30}$$

where

$$\begin{aligned} \frac{\partial^2 F}{\partial C_{L_1}^2} &= 2\pi\big(12C_{L_1}^2A_{L_1}+8C_{L_2}^2A_{L_1,L_2}+\Lambda_{L_1}B_{L_1}\big), \\ \frac{\partial^2 F}{\partial C_{L_2}^2} &= 2\pi\big(12C_{L_2}^2A_{L_2}+8C_{L_1}^2A_{L_1,L_2}+\Lambda_{L_2}B_{L_2}\big), \\ \frac{\partial^2 F}{\partial C_{L_1}C_{L_2}} &= 32\pi C_{L_1}C_{L_2}A_{L_1,L_2}. \end{aligned} \tag{2.31}$$

For giant vortex states, we can rewrite these stability equations into a simple form:

i) for the case $C_{L_1}^{(0)}=0$ and $C_{L_2}^{(0)}\neq 0$,

$$\begin{aligned} \frac{\partial^2 F}{\partial C_{L_1}^2}\Big|_{C_{L_1}=0,C_{L_2}=C_{L_2}^{(0)}} &= \frac{8\pi}{A_{L_2}}\big(\Lambda_{L_1}A_{L_2}B_{L_1}-2\Lambda_{L_2}A_{L_1,L_2}B_{L_2}\big)>0, \\ \frac{\partial^2 F}{\partial C_{L_2}^2}\Big|_{C_{L_1}=0,C_{L_2}=C_{L_2}^{(0)}} &= -16\pi\Lambda_{L_2}B_{L_2}>0, \end{aligned} \tag{2.32a}$$

ii) for the case $C_{L_1}^{(0)}\neq 0$ and $C_{L_2}^{(0)}=0$,

$$\begin{aligned} \frac{\partial^2 F}{\partial C_{L_2}^2}\Big|_{C_{L_1}=C_{L_1}^{(0)},C_{L_2}=0} &= \frac{8\pi}{A_{L_1}}\big(\Lambda_{L_2}A_{L_1}B_{L_2}-2\Lambda_{L_1}A_{L_1,L_2}B_{L_1}\big)>0, \\ \frac{\partial^2 F}{\partial C_{L_1}^2}\Big|_{C_{L_1}=C_{L_1}^{(0)},C_{L_2}=0} &= -16\pi\Lambda_{L_1}B_{L_1}>0. \end{aligned} \tag{2.32b}$$

The free energy of a giant vortex state is

$$\boxed{F_{L_i} = -2\pi\Lambda_{L_i}^2 \frac{B_{L_i}^2}{A_{L_i}},\ \ i = 1, 2.} \tag{2.33}$$

And the superconducting current is the same as Eq. (2.18).

For multivortex states, we need to do some numerical calculation to determine the stability. The Gibbs free energy is

$$\boxed{F_{L_1,L_2} = 2\pi \frac{-\Lambda_{L_1}^2 A_{L_2} B_{L_1}^2 - \Lambda_{L_2}^2 A_{L_1} B_{L_2}^2 + 4\Lambda_{L_1}\Lambda_{L_2} A_{L_1,L_2} B_{L_1} B_{L_2}}{A_{L_1} A_{L_2} - 4A_{L_1,L_2}^2}.} \tag{2.34}$$

The superconducting current can be obtained in a similar way as for the case of the giant vortex states. Substitute the two-component order parameter Ψ into Eq. (2.17), we have the current expression

$$\begin{aligned} \vec{j}_s &= \Big\{ (\frac{L_1}{\rho} - \frac{H\rho}{2})(C_{L_1}^{(0)})^2 \psi_{L_1}^2 + (\frac{L_2}{\rho} - \frac{H\rho}{2})(C_{L_2}^{(0)})^2 \psi_{L_2}^2 \\ &\quad + (\frac{L_1 + L_2}{\rho} - H\rho) C_{L_1}^{(0)} C_{L_2}^{(0)} \psi_{L_1} \psi_{L_2} cos[(L_2 - L_1)\varphi] \Big\} \vec{e}_\varphi. \end{aligned} \tag{2.35}$$

2.3 VORTICITY

Different superconducting states (giant vortex states and multivortex states) can nucleate when a particular magnetic field is applied to a mesoscopic sample (Refs. [1] and [11]). These states have different free energies and different vortex configurations, and they can be characterized by a **vorticity** L.

While we go along the boundary of the circular cone in the plane $z{=}z_0$, if the phase of the order parameter changes by $L \times 2\pi$, then we say this superconducting state has a vorticity valued L.

For a giant vortex state, the vorticity L is the angular momentum quantum number of its order parameter. And for a multivortex state, whose order parameter is constructed by two components with angular momentum quantum numbers L_1 and L_2, the vorticity is equal to the maximum of L_1 and L_2. This is similar to what happens in a mesoscopic thin disk (Ref. [1]) and a mesoscopic sphere (Ref. [11]). We will show the corresponding results in the following chapters.

3

Giant Vortex States

In this chapter we numerically study the giant vortex states in a superconducting mesoscopic circular cone with the software packages Matlab and Comsol according to the theoretical formalism described in section 2.1. For a given vorticity L and a given magnetic field H, we use Matlab and Comsol to solve Eq. (2.8). Moreover, we construct a vorticity distribution diagram, eigenvalue-magnetic field diagram (Λ-H) and free energy-magnetic field diagram (F-H), the Cooper-pair density distribution, and the phase distribution of the order parameter.

3.1 LARGEST VORTICITY DISTRIBUTION DIAGRAM

To find the dependence of the superconducting states on the size of the circular cone, it is necessary to know the relation between the largest allowed vorticity of the giant vortex states (which is the largest angular momentum quantum number L with a **negative** eigenvalue for the operator $\hat{L}$ for a certain circular cone at any value of the applied magnetic field) and the size of the circular cones. For giant vortex states the stability condition requires a negative eigenvalue. The vorticity distribution diagram is a diagram that gives the largest allowed vorticity of different circular cones.

In Fig. 3.1, we show two vorticity distribution diagrams. In Fig. 3.1(a) circular cones are described by height z_0 (from 0.1ξ to 6ξ, $\Delta z_0 = 0.1\xi$) and its vertex angle θ (from 1° to 60°, $\Delta\theta = 1^\circ$). The same information is given in

Fig. 3.1(b) but now as a function of the height z_0 (from 0.1ξ to 6ξ, $\Delta z_0 = 0.1\xi$) and its radius r (from 0.1ξ to 6ξ, $\Delta r = 0.1\xi$).

From these two plots, we learn that: (1) circular cones with larger vertex angle and height have a giant vortex state with larger vorticity, i.e. there are more vortex states corresponding to negative eigenvalues for larger size; (2) circular cones with larger radius and height have a giant vortex state with larger vorticity; (3) increasing the height or the vertex angle increases L; (4) while the height of a circular cone is constant and the radius increases, the increment of the largest vorticity is much larger than that in the opposite case; (5) in both plots, the Meissner region, i.e. with L=0, has a large area which corresponds to the small size of circular cones.

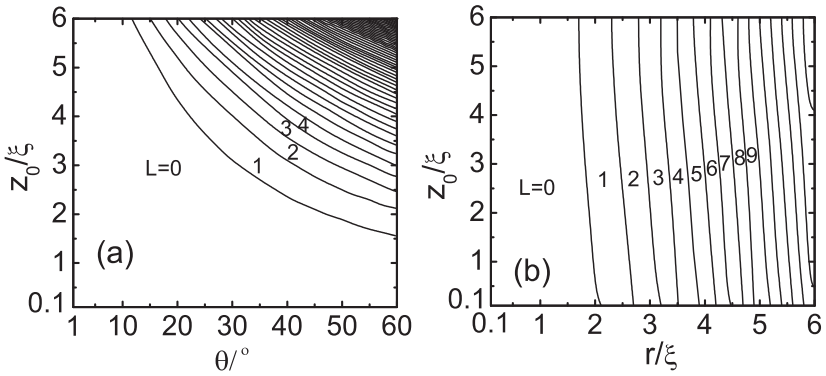

Fig. 3.1 The largest vorticity which is able to nucleate in the circular cone.

3.2 EIGENVALUE, FREE ENERGY AND GROUND STATE

Here we show the Λ-H diagrams for four circular cones with parameters (z_0, θ, r): (2.5ξ, 30°, 1.44ξ) (which has only L=0), (2.5ξ, 45°, 2.5ξ) (which has the largest vorticity of L=2), (4ξ, 45°, 4ξ) (which has the largest vorticity of L=6), (2.5ξ, 60°, 4.33ξ) (which has the largest vorticity of L=7)(see Fig. 3.2). The dotted horizonal line corresponds to the $\Lambda = 0$ level. From these plots one can see the effect of increasing the largest vorticity: (i) more vortex states appear, i.e. the number of possible solutions (with negative eigenvalues) of Eq. (2.8) (n=0) increases; (ii) the magnetic-field range over which solutions of Eq. (2.8) (n=0) with negative eigenvalues can be found decreases.

The expression of the free energy is obtained as Eq. (2.14). In Fig. 3.3, we show F-H diagrams for cones the (2.5ξ, 30°, 1.44ξ), (2.5ξ, 45°, 2.5ξ), (4ξ, 45°, 4ξ), (2.5ξ, 60°, 4.33ξ). The dotted horizontal line in Fig. 3.3 corresponds to the $F/F_0 = 0$ level, where $F_0 = \alpha^2/2\beta$.

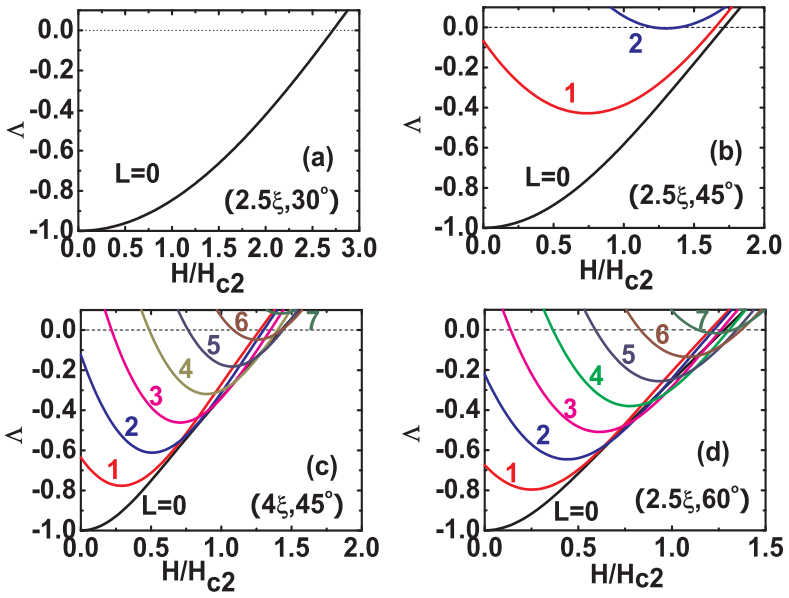

Fig. 3.2 Eigenvalue vs. magnetic field plots for different circular cones (z_0, θ, r): (a) (2.5ξ, 30°, 1.44ξ), (b) (2.5ξ, 45°, 2.5ξ), (c) (4ξ, 45°, 4ξ), (d) (2.5ξ, 60°, 4.33ξ).

For a certain magnetic field it is possible to have giant vortex states with different vorticities. The state with the lowest free energy through the whole region is called the **ground state**, and the others are **meta-stable states**. With increasing magnetic field the ground state will transit from L→L+1 when the curves of these two states cross each other. With increasing the value of largest vorticity of circular cones, these crossing points shift towards lower magnetic field and the superconducting/normal transition field decreases. These results are similar to those found in Ref. [11] for superconducting spheres. In Fig. 3.4, we show the vorticity of the ground states vs. the applied magnetic field for the circular cones (z_0=4ξ, θ=45°, r=4ξ) and (z_0=2.5ξ, θ=60°, r≈ 4.33ξ).

3.3 COOPER-PAIR DENSITY AND THE PHASE OF THE ORDER PARAMETER

Now, we investigate the Cooper-pair density of the different giant vortex states which is given by the following relation due to the expression of the order parameter Eq. (2.16)

$$|\Psi(\rho,\varphi,z)|^2 = -\Lambda\frac{I_2}{I_1}\psi_L(\rho,z)^2. \tag{3.1}$$

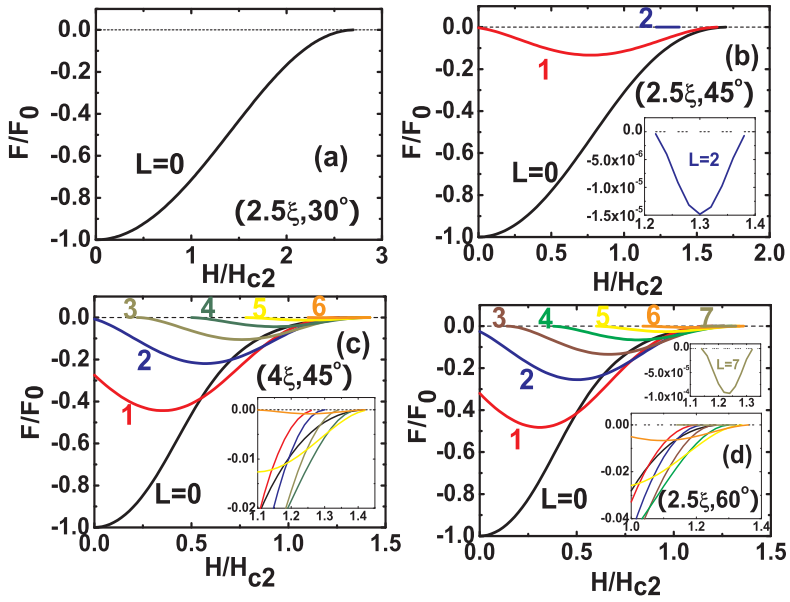

Fig. 3.3 The Gibbs free energy vs. the applied magnetic field plots for circular cones (z_0, θ, r): (a) (2.5ξ, 30°, 1.44ξ), (b) (2.5ξ, 45°, 2.5ξ), (c) (4ξ, 45°, 4ξ), (d) (2.5ξ, 60°, 4.33ξ).

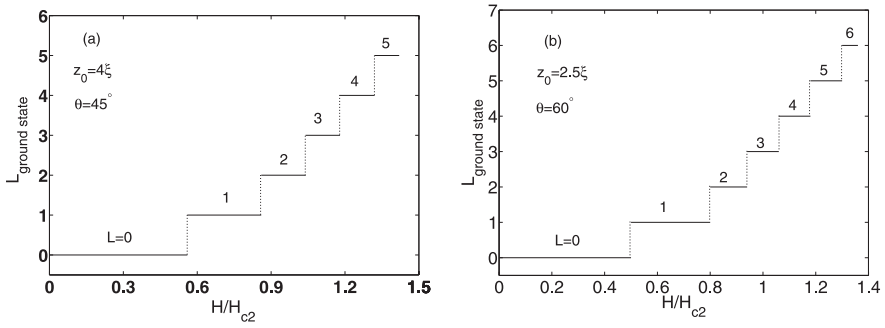

Fig. 3.4 The vorticity of the ground state vs. the applied magnetic field plots for circular cones (z_0, θ, r): (a) (4ξ, 45°, 4ξ), (b) (2.5ξ, 60°, 4.33ξ).

In Fig. 3.5 Cooper-pair densities of giant vortex states in the circular cone (4ξ, 45°, 4ξ) with different parameters (L=0,1,2 and H=0.1H_{c2}, 0.6H_{c2}, 1H_{c2}) are shown. Notice that the stable giant vortex states should have negative eigenvalues for the operator $\hat{L}$, when we only consider one component in the expression of the order parameter Ψ.

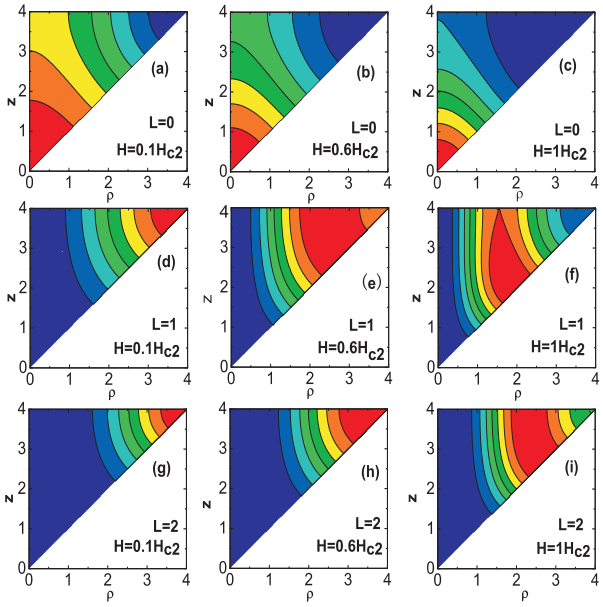

Fig. 3.5 The Cooper-pair density distribution in the ρ-z plane (where ρ=$\sqrt{x^2+y^2}$) for a circular cone (4ξ, 45°, 4ξ) for different magnetic fields and vorticity: H/H_{c2}=0.1, 0.6, 1, (a, b, c) L=0, (d, e, f) L=1, (g, h, i) L=2. High Cooper-pair density is marked by red color, while low Cooper-pair density is marked by blue color. According to Fig. 3.4 the states of plots (a, e, i) are the ground state.

To study the detail how the applied magnetic field will affect the Cooper-pair density of the giant vortex states, we plot the Cooper-pair density of giant vortex states L=1 and L=2 in the z=z_0 plane for the circular cone (z_0=4ξ, θ=45°, r=4ξ) at different applied fields in Fig. 3.6. The profiles here are similar with the results for the thin disk shown in Ref. [6].

According to Fig. 3.5 for the Meissner state $L = 0$ there is no vortex in the cone. The high Cooper-pair density is found around the z axis, while the highest region is located at the vertex. This is a consequence of surface superconductivity, i.e. superconductivity is enhanced when the superconductor is comparable or smaller than ξ (Ref. [17]). Because near the vertex the size of the cone is smaller than the coherence length ξ, the Cooper-pair density there will change little. With increasing the field the Meissner state is suppressed and is moving towards the z axis and the vertex. For $L > 0$, the vortex is situated along the z axis ($|\Psi|^2$=0, for ρ=0 and $z \in [0, z_0]$). When the applied magnetic field is not very strong (see Figs. 3.5(d)(g)), the highest Cooper-pair density is found around the region $(z, \rho) \sim (z_0, z_0 tan(\theta))$. For giant vortex states ($L > 0$) when the applied magnetic field is not very strong the highest Cooper-pair density is found around the region $z = z_0$ and $\rho = z_0 tan(\theta)$.

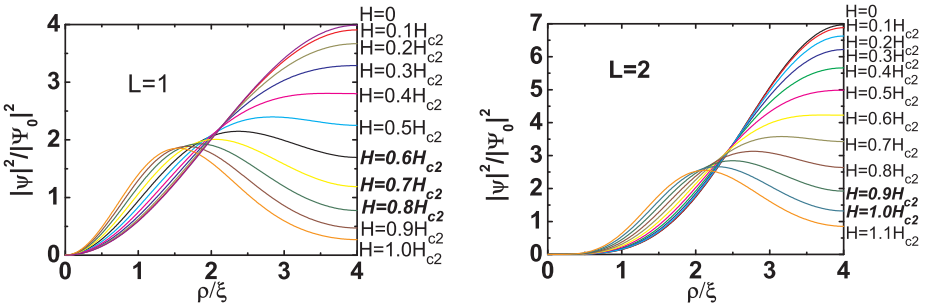

Fig. 3.6 The Cooper-pair density of giant vortex states L=1 (a) and L=2 (b) in the z=4ξ plane (where ρ=$\sqrt{x^2+y^2}$) for the circular cone (z_0=4ξ, θ=45°, r=4ξ) for different magnetic fields. According to Fig. 3.4 the states of curves H/H_{c2}=0.6, 0.7, 0.8 in plot (a) and the states of curves H/H_{c2}=0.9, 1 in plot (b) are the ground state.

When the applied magnetic field is sufficiently strong the highest Cooper-pair density will go deeply into the cones (see Figs. 3.5(c,f,i) and Fig. 3.6). With increasing field, the vortex along the z-axis is suppressed and its radius becomes smaller, and the region of the highest Cooper-pair density is also suppressed and is moving towards the vertex along the generatrix. With increasing vorticity, at a certain applied magnetic field the vortex along the vertex becomes larger. It seems that larger vorticity is much more difficult to be suppressed.

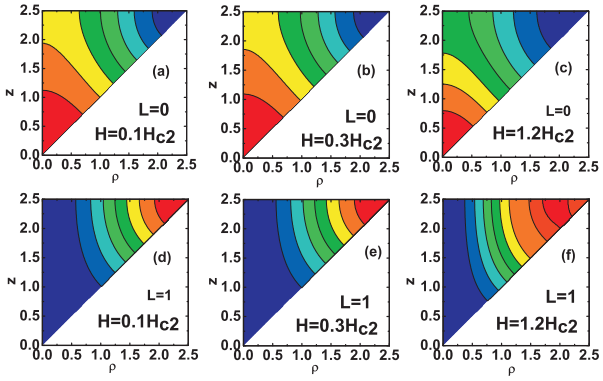

Fig. 3.7 The Cooper-pair density distribution in the ρ-z plane (where ρ=$\sqrt{x^2+y^2}$) for a circular cone (2.5ξ, 45°, 2.5ξ)(a,b,c:L=0; d,e,f:L=1) for different magnetic fields (H/H_{c2}=0.1, 0.3, 1.2). High Cooper-pair density is marked by red color, while low Cooper-pair density is marked by blue color. For this circular cone, the ground state is Meissner state L=0 according to Fig 3.3(b).

Here we show some Cooper-pair density distribution diagrams (in the ρ-z plane) for giant vortex states ($L=0,1$) in the cone with parameters (z_0, θ, r):

(2.5ξ, 45°, 2.5ξ) in Fig. 3.7, and (2.5ξ, 60°, 4.33ξ) in Fig. 3.8 at the applied magnetic fields (H/H_{c2}=0.1, 0.3, 1.2).

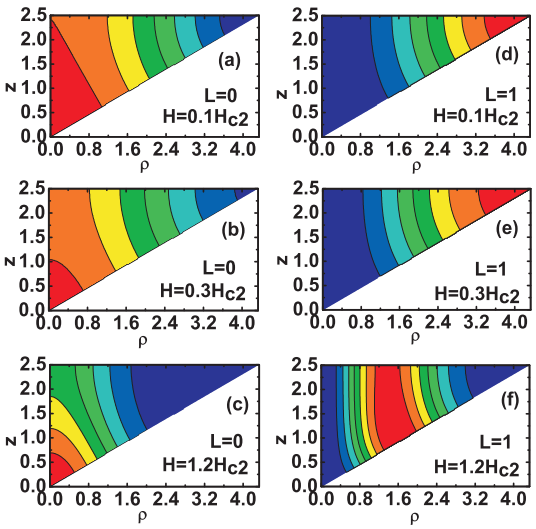

Fig. 3.8 The Cooper-pair density distribution in the ρ-z plane (where ρ=$\sqrt{x^2+y^2}$) of the circular cone (2.5ξ, 60°, 4.33ξ) (a,b,c: L=0; d,e,f: L=1) for different magnetic fields (H/H_{c2}=0.1, 0.3, 1.2). High Cooper-pair density is marked by red color, while low Cooper-pair density is marked by blue color.

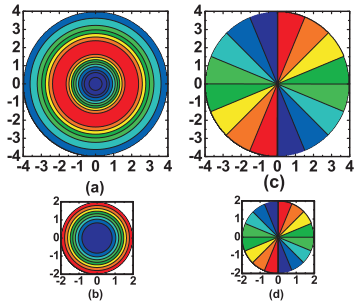

Fig. 3.9 The Cooper-pair density and the phase of order parameter in the planes at z=z_0 and z=$z_0/2$ for the circular cone (4ξ, 45°, 4ξ) at applied magnetic field H=1.2H_{c2} with vorticity L=2. For (a) and (b) high Cooper-pair density is marked by red color, while low Cooper-pair density is marked by blue color. For (c) and (d) blue region indicates phase near 0, while red region indicates phase near 2π.

Now, we consider the phase of the order parameter, which can be given by the following expression (Eq. (2.16)). We can see that the phase of the order parameter at a point (ρ, φ, z) is vorticity times the angle φ, i.e. $L \times \varphi$. So,

for a giant vortex state with vorticity L, while going around the center of the vortex, the phase of the order parameter changes always with $2\pi L$. In Fig. 3.9 the Cooper-pair density distributions and their relevant distributions of the phase of the order parameter in the $z = z_0$ and $z = z_0/2$ planes are shown for the circular cone (z_0=4ξ, θ=45°, r=4ξ) with L=2 and H=1.2H_{c2}.

3.4 EXCITED STATES

Here we call the states with eigenfunctions $\psi_{L,n}$ (where $n \neq 0$) of the LGL equation as excited states. With larger n, the corresponding eigenvalue is larger for a fixed angular momentum quantum number L. In the last chapters only the states with lowest eigenvalues ($n = 0$) are considered, now we investigate the case for excited states.

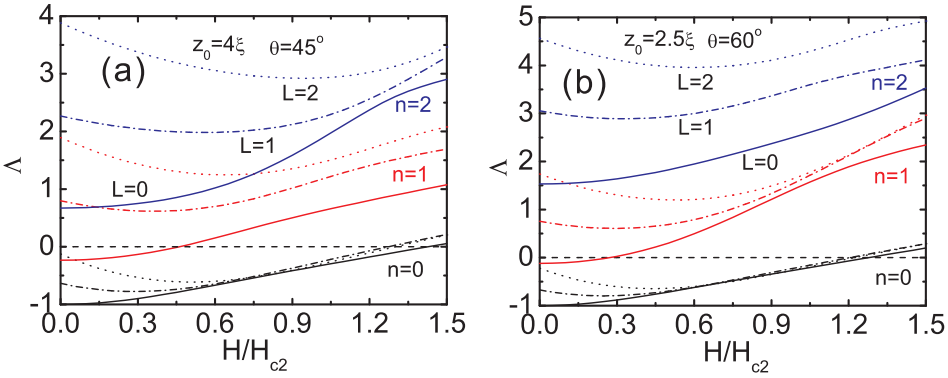

Fig. 3.10 The eigenvalue Λ as a function of the applied magnetic field for the states with L=0 (solid curves), L=1 (dotted dashed curves) and L=2 (dotted curves) corresponding to the lowest eigenvalue (black curves), the first excited state (red curves) and the third excited state (blue curves). The dashed horizontal lines correspond to the Λ=0 level. Fig. (a) is for the circular cone (z_0=4ξ, θ=45°, r=4ξ), while Fig. (b) is for circular cone (z_0=2.5ξ, θ=60°, r$\approx$ 4.33ξ).

In Fig. 3.10, we show the magnetic dependence of the eigenvalue for the states with vorticities L=0,1,2 and n=0,1,2 for the circular cones: (z_0=4ξ, θ=45°, r=4ξ) and (z_0=2.5ξ, θ=60○, r$\approx$ 4.33ξ). The dashed horizontal lines in the figures correspond to the Λ=0 level. In Fig. 3.10(a) and Fig. 3.10(b) we use the following conventions: (i) the black curves (except the dashed horizontal lines) correspond to the states with n=0; (ii) the red curves correspond to the states with n=1; (iii) the blue curves correspond to the states with n=2; (iv) the solid curves correspond to the states with L=0; (v) the dashed dotted curves correspond to the states with L=1; (vi) the dotted curves correspond to the states with L=2. We can learn form these two figures that only the excited state with n=1 and L=0 has a negative eigenvalues in the low applied

magnetic field region. According to the stability condition of the giant vortex states, only the states with negative eigenvalues are (mete-)stable. So, for these circular cones only the excited state (L=0, n=1) may exist when the magnetic field is sufficiently low.

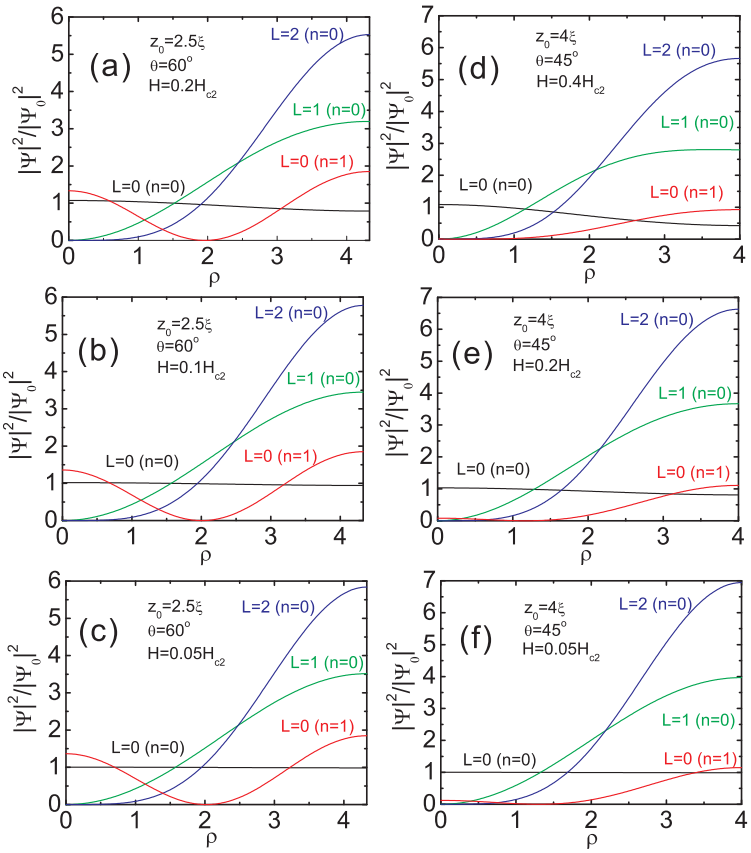

Fig. 3.11 The profiles of the Cooper-pair density of the giant vortex states (L,n): (0,0), (0,1), (1,0) and (2,0) in the plane z=z_0 for circular cones (z_0=2.5ξ, θ=60○, r≈ 4.33ξ) and (z_0=4ξ, θ=45°, r=4ξ) at different applied magnetic fields. Figures (a,b,c) are for the circular cone (z_0=2.5ξ, θ=60○, r≈ 4.33ξ), while figures (d,e,f) are for the circular cone (z_0=4ξ, θ=45○, r=4ξ). At these applied magnetic fields the first excited state (L=0, n=1) always has a negative eigenvalue.

Next, we plot the profiles of the Cooper-pair density of the giant vortex states (L,n): (0,0), (0,1), (1,0) and (2,0) in the plane z=z_0 for these two circular cones at different applied magnetic fields in Fig. 3.11. At these applied magnetic fields the first excited state (L=0, n=1) always has a negative eigenvalue. From these figures we can see that: (i) the Cooper-pair density of the first excited state (L=0,n=1) vanishes inside the cone. This phenomenon

is similar with what happens in a thin disk (see Ref. [1]); (ii) the first excited state (L=0, n=1) is difficult to be suppressed with increasing applied magnetic field. In Fig. 3.12, we shoe the Cooper-pair density distributions of the state (L=0, n=1) at the applied magnetic field H/H_{c2}=0.05 for the circular cone (z_0=4ξ, θ=45°, r=4ξ) in the ρ-z plane (ρ=$\sqrt{x^2+y^2}$) and in the z=z_0 plane.

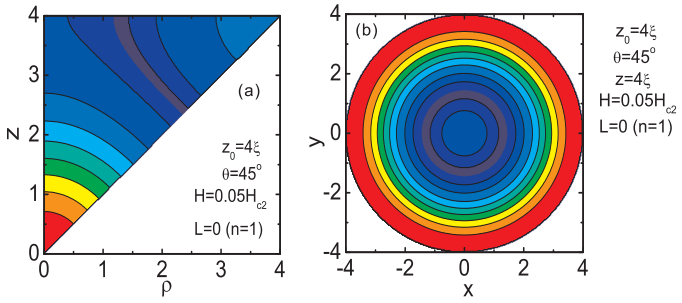

Fig. 3.12 The Cooper-pair density distributions of the first excited state (L=0, n=1) at the applied magnetic field H/H_{c2}=0.05 for the circular cone (z_0=4ξ, θ=45°, r=4ξ) in the ρ-z plane (where ρ=$\sqrt{x^2+y^2}$) and in the z=z_0 plane. The Cooper-pair density in the navy region is lower than 5×10^{-3}. High Cooper-pair density is marked by red, while low density is marked by blue.

4
Multivortex States

In this chapter, we will investigate the multivortex states for circular cones with different heights z_0 and vertex angles 2θ (or radius r). It is known that with increasing size of the superconducting sample the giant vortex states will decay into many single vortices. This is the so-called *multivortex* state which can be described as a combination of solutions of Eq. (2.8).

Here we only consider states where the order parameter is a linear combination of only two components. The expressions of the free energy F, the coefficients (C_{L_1}, C_{L_2}) and the order parameter Ψ of the multivortex states have been given in Section 2.2. The stability of the multivortex states and the giant vortex states is determined by their stability conditions Eq. (2.30) and Eq. (2.32). We are interested in the free energy vs. magnetic field diagrams and the vortex configuration (under the condition that the magnetic field and the combination are fixed) for different circular cones. In this thesis, we use (L_1, L_2) to indicate the multivortex state whose order parameter is formed by ψ_{L_1} and ψ_{L_2}, while L for the giant vortex state with vorticity L.

4.1 FREE ENERGY AND GROUND STATE

First, we give the free energy of the (meta-)stable states as a function of the applied magnetic field for circular cones with parameters (z_0, θ, r): (2.5ξ, 45°, 2.5ξ), (4ξ, 45°, 4ξ), (2.5ξ, 60°, 4.33ξ). The curves in the (F-H) diagrams (except the horizontal line F=0) are *the meta-stable state* and *the ground states*. The values of the free energy for the giant vortex states and the

multivortex states are given by Eq. (2.33) and Eq. (2.34). The ground state corresponds to the lowest curve with smallest free energy, while the meta-stable states correspond to the other curves.

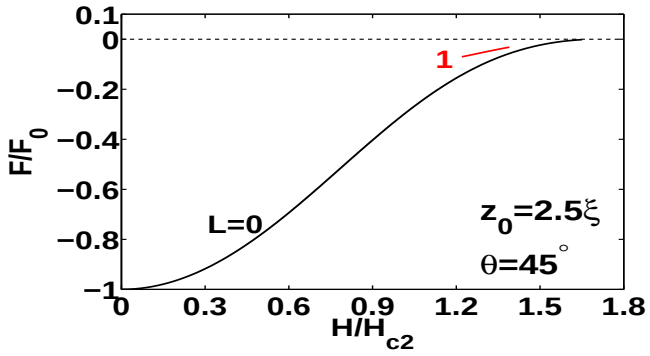

Fig. 4.1 The free energy of the (meta-) stable states for the circular cone with parameters (z_0=2.5ξ, θ=45°, r=2.5ξ) as a function of the applied magnetic field.

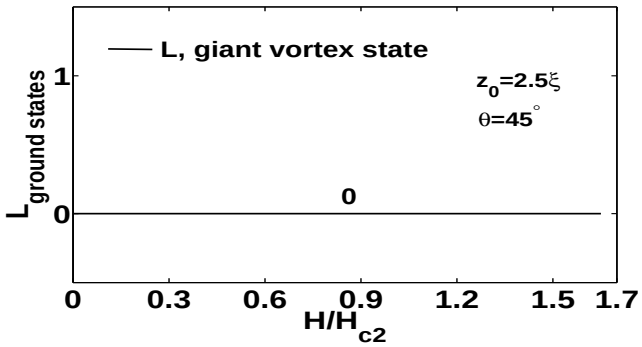

Fig. 4.2 The vorticity of the ground state for the circular cone with parameters (z_0=2.5ξ, θ=45°, r=2.5ξ) as a function of the applied magnetic field.

In Fig.4.1, we show the free energy of the (meta-) stable states for the circular cone with parameters (z_0=2.5ξ, θ=45°, r=2.5ξ) as a function of the applied magnetic field. There is no (meta-)stable multivortex state that can nucleate for this circular cone. The giant vortex states L are given by solid curves in the figure. The horizontal dashed line is F=0. Notice that we know that the largest allowed vorticity of the giant vortex states for this circular cone is 2. The giant state (L=2) disappears here. The region of the meta-stable giant state (L=1) is narrower than that in Fig. 3.3(b). The region of

the Meissner state (L=0) is the same as that in Fig. 3.3(b). The reason can be find in the stability conditions Eq. (2.32).

In Fig.4.2, the vorticity of the ground state for the circular cone (z_0=2.5ξ, θ=45°, r=2.5ξ) is shown as a function of the applied magnetic field. Obviously, the vorticity of the ground state is a constant and equal to zero in the whole region. And the ground state is the Meissner state (L=0).

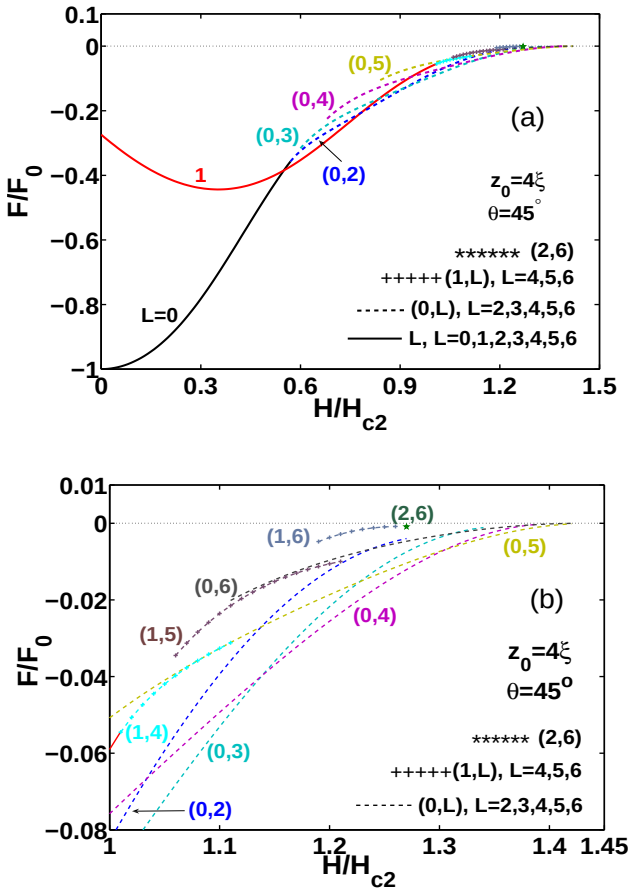

Fig. 4.3 The free energy of the (meta-) stable states for the circular cone with parameters (z_0=4ξ, θ=45°, r=4ξ) as a function of the applied magnetic field. Fig. (a) is for the whole region of the field, while Fig. (b) is for the high filed region.

In Fig. 4.3, we show the free energy of the (meta-)stable states for the circular cone with parameters (z_0=4ξ, θ=45°, r=4ξ) as a function of the applied magnetic field. A zoom of the hight field region is shown in Fig. 4.3(b). The giant vortex states L are given by solid curves, the multivortex states are given by dashed and dotted curves. The horizontal dotted line

stands for F=0. From the last chapter, we know that the largest vorticity of giant vortex states for this circular cone is 6. We are interested in the multivortex states, so when the curves of multivortex states and giant vortex states overlaps, the curves of the giant vortex states will then not be shown in the figure.

The following states are stable for this circular cone:

(i) the giant vortex states L, L=0-6;

(ii) the multivortex states (0,L), L=2-6; (1,L), L=4-6; (2,L), L=6.

For the multivortex states with vorticity L=4, the (0,4) state has lower free energy than the (1,4) state in their common magnetic field region, and the (1,4) state has lower free energy than the (2,4) state in their common magnetic field region. For the multivortex states with vorticity L=5, the (0,5) state has lower free energy than the (1,5) state which has lower free energy than the (2,5) state. There are no magnetic field points where the multivortex states with the same vorticity nucleate in this circular cone.

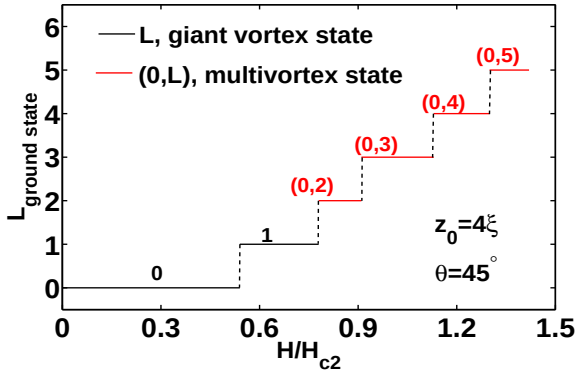

Fig. 4.4 The vorticity of the ground state for the circular cone with parameters (z_0=4ξ, θ=45°, r=4ξ) as a function of the applied magnetic field.

In Fig. 4.4, we show the vorticity of the ground state for the circular cone with parameters (z_0=4ξ, θ=45°, r=4ξ) as a function of the applied magnetic field. When the applied magnetic field increases, the vorticity of the ground state will go from 0 to 5. The ground state is mixed by the giant vortex states (L=0-5) and the multivortex states (0,L) where L=2-5. There is no giant vortex state (L=6) and other multivortex states existing in the ground state. Notice that near the superconducting/normal boundary we have a multivortex state while in a superconducting disk this is usually a giant vortex state.

In Fig. 4.5, we give the free energy of the (meta-)stable states for the circular cone with parameters (z_0=2.5ξ, θ=60°, $r \approx 4.33\xi$) as a function of the applied magnetic field. From the last chapter, we know that the largest

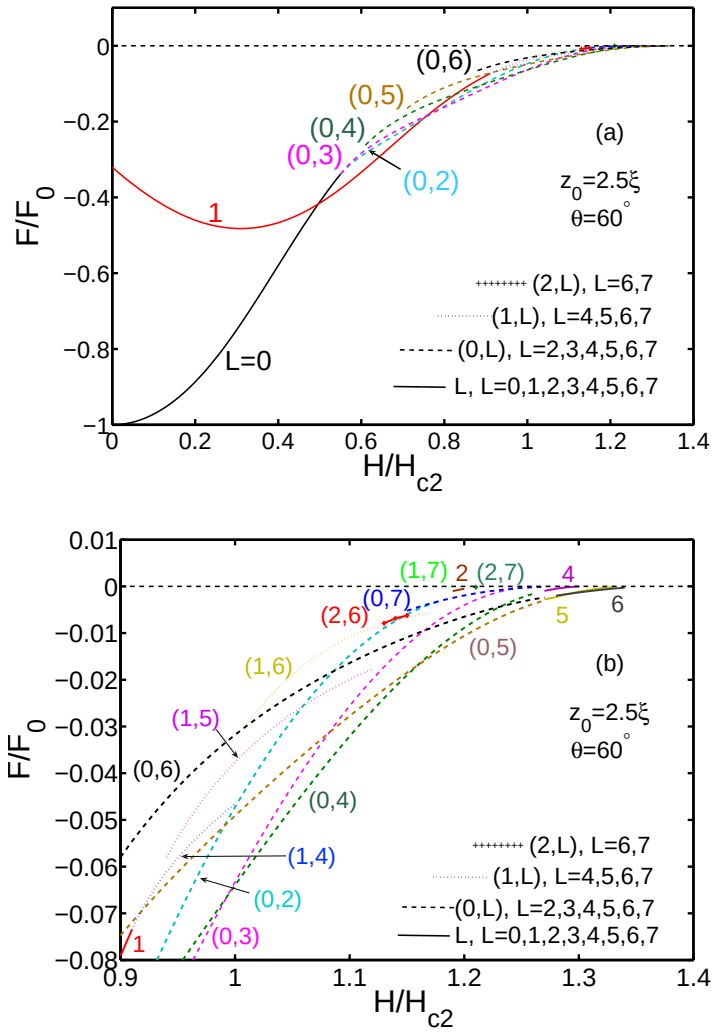

Fig. 4.5 The free energy of the (meta-)stable states for the circular cone with parameters (z_0=2.5ξ, θ=60°, r≈ 4.33ξ) as a function of the applied magnetic field. Fig. (a) is for the whole region of the field, while Fig. (b) is for the high filed region.

vorticity of the giant vortex states for this circular cone is equal to 7. Fig. 4.5(a) is for the whole magnetic field region, while Fig. 4.5(b) is for the high magnetic field region. The curves of giant vortex states, which overlap with the curves of the multivortex states, are not shown in the figure. The giant vortex states L are given by solid curves, the (1,L) states by dashed curves with star mark, the (2,L) states by dashed curves with plus mark.

We can find that the giant vortex states stabilize for L=0 up to 7. The (0,L) states stabilize for L=2-7, the (1,L) states for L=4-7, the (2,L) states for L=6-7.

Now, we focus on the multivortex states which have the same vorticity. For the states (0,6), (1,6) and (2,6), they have the same vorticity which is equal to 6. In their common magnetic field region, the (0,6) state has a lower free energy than the (1,6) state, and the (1,6) state has a lower free energy than the (2,6) state. For the states (0,4) and (1,4), in their common field region the (0,4) state has a lower free energy than the (1,4) state. For the states (0,5) and (1,5), in their common field region the (0,5) state has a lower free energy than the (1,5) state. For the states (0,7), (1,7), in their common magnetic field region the (0,7) state has a lower free energy than the (1,7) state. There is no common field region for states (1,7) and (2,7).

In Fig. 4.5(b) we also could see that the states (0,6) and (1,6) can nucleate at H=1.01H_{c2} and the states (1,6) and (2,6) can nucleate at H=1.13H_{c2}. These three multivortex states have the same vorticity.

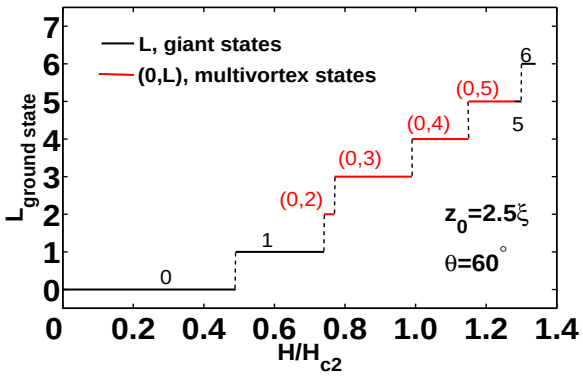

Fig. 4.6 The vorticity of the ground state for the circular cone with parameters (z_0=2.5ξ, θ=60°, r≈ 4.33ξ) as a function of the applied magnetic field.

In Fig. 4.6, the vorticity of the ground state for the circular cone (z_0=2.5ξ, θ=60°, r≈ 4.33ξ) is given as a function of the applied magnetic field. With increasing magnetic field, the vorticity of the ground state increases from 0 to 6. And the ground state is mixed by the giant vortex states (L=0-6) and the multivortex states (0,L) where L=2-5. There is no giant vortex state (L=7) and other multivortex states nucleating as ground state.

At the end of this section, we investigate the ground state of circular cones with parameters (z_0=4, θ=1°-60°, r=z_0 × $tan(\theta)$). In Fig. 4.7, we show the vorticity of the ground states for such circular cones as a function of the applied magnetic field. Notice that the height of these circular cones is fixed

and equal to 4ξ. In Fig. 4.7(a), we find that when the half opening angle is smaller than 30° the ground state is Meissner state. The region with color is the states with vorticity larger than zero. In Fig. 4.7(b), we show the detail of this region. In Fig. 4.7(c), we show the components of the ground state, i.e. identify the regions of giant vortex states and multivortex states. When the applied magnetic field is quite small, the ground state is giant vortex state. With increasing magnetic field the ground state is multivortex state. Normally, before the superconductivity disappear the ground state will be giant vortex state again except the case in the region around θ=43° and H/H_{c2}=1.4. In this region the ground state will become normal state without going through the giant vortex state.

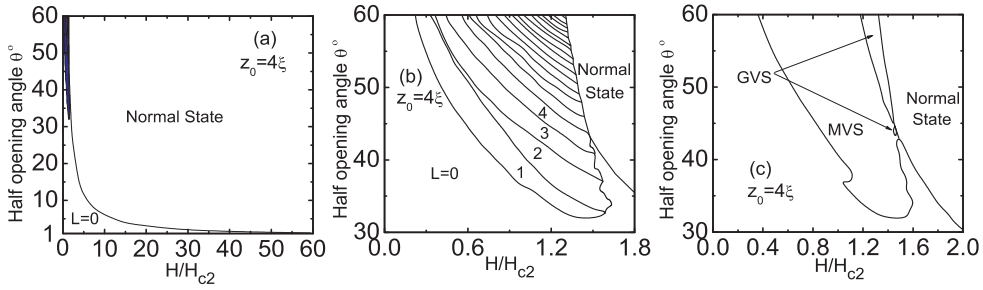

Fig. 4.7 The phase diagram of the ground state for the circular cones with parameters (z_0=4ξ, θ=1°-60°, r=$z_0 \times tan(\theta)$). The region marked by color in plot (a) is the states with vorticity larger than zero. A zoom of this region is shown in plot (b). In plot (c) the situation of the composition of the ground state is shown.

4.2 COOPER-PAIR DENSITY AND THE PHASE OF THE ORDER PARAMETER

Now, we study the structures of the Cooper-pair density and the phase of the corresponding order parameter for the (meta-)stable multivortex states and the effects of changing the applied magnetic field. All of this work is based on the expression of the order parameter for the multivortex states which is obtained in Section 2.2 (Eq. (2.23) and Eq. (2.29)).

First, we investigate the structures of the (meta-)stable multivortex states for the circular cone (z_0=4ξ, θ=45°, r=4ξ). From the last section, we know that all the (meta-) stable multivortex states for this cone are (0,L) L=2-6, (1,L) L=4-6 and (2,6) states. In Fig. 4.8 and Fig. 4.9, we show the plots of the vortex configuration, the Cooper-pair density and the phase of the corresponding order parameter for these multivortex states. In Fig. 4.8 there are five rows. Each row has seven pictures. The first one is the vortex configuration, the others are plots of the Cooper-pair density and the phase

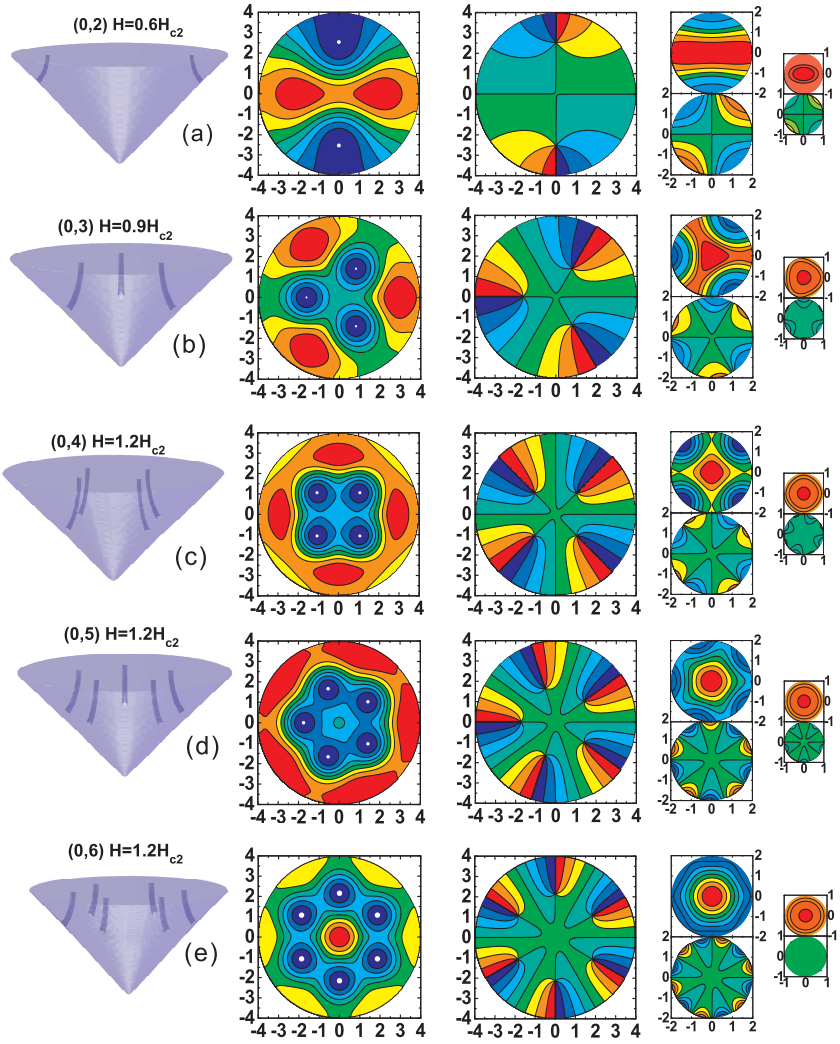

Fig. 4.8 Plots of the vortex configuration, Cooper-pair density and the phase of the order parameter of the (meta-)stable multivortex states (0,L) L=2-6 at the applied magnetic fields H/H_{c2}=0.6, 0.9, 1.2 for the circular cone (z_0=4ξ, θ=45°, r=4ξ). The Cooper-pair density and the phase of the order parameter are shown in the z = 4ξ, 2ξ, ξ planes.

of the order parameter in the z=4ξ, 2ξ, ξ planes. In Fig. 4.9 there are four rows. Each row has five pictures. The first one is the vortex configuration, the others are plots of the Cooper-pair density and the phase of the order parameter in the z=4ξ, 2ξ planes.

There are many rows in Fig. 4.8 and Fig. 4.9. Each row has seven pictures, the first one is the vortex configuration, the others are plots of the Cooper-pair density and the phase of the order parameter in the z=4ξ, 2ξ, ξ planes.

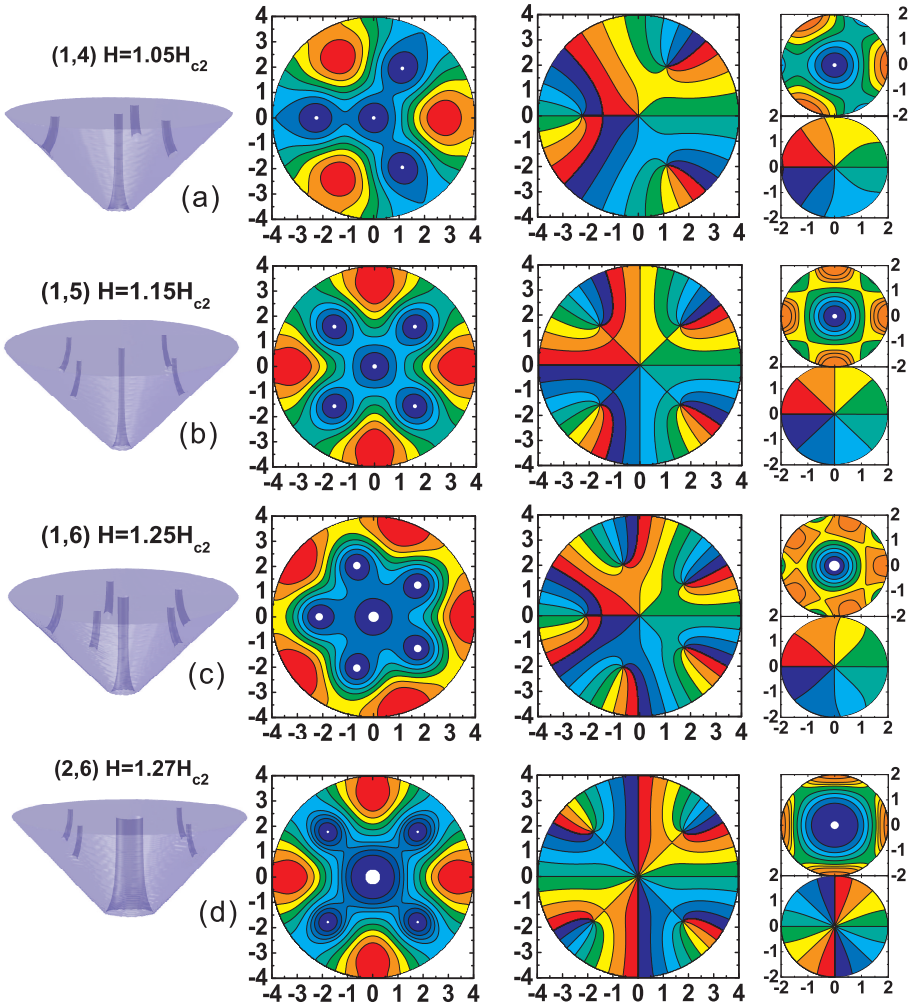

Fig. 4.9 The plots of the vortex configuration, Cooper-pair density and the phase of order parameter of the (meta-)stable multivortex states (1,L) L=4-6 and (2,6) at the applied magnetic fields H/H_{c2}=1.05, 1.15, 1.25, 1.27 for the circular cone (z_0=4ξ, θ=45°, r=4ξ). The Cooper-pair density and the phase of the order parameter are shown in the $z = 4\xi$, 2ξ planes.

It is necessary to mention that the meaning of the same color are different in the plots of Cooper-pair density and the phase of the order parameter. In

the plots of Cooper-pair density, the red region stands for high density, while the blue stands for low density. The white hole stands for the region where the Cooper-pair density is lower than 10^{-3} except that in Fig. 4.9(d) which is lower than 10^{-4}. In the plots of the phase of the order parameter the region in which the phase is very small and near zero is given by blue, while the region with phase near 2π is marked by red. The boundary of blue and red region is the place with phase equal to zero (or 2π). In the plots of the vortex configuration, the values of the iso-surface are different and lower than 10^{-3}. In Fig. 4.9(d) the value of the iso-surface for the (2,6) state is 5×10^{-4}. From the plot of the order parameter we also can find the locations of the vortices clearly.

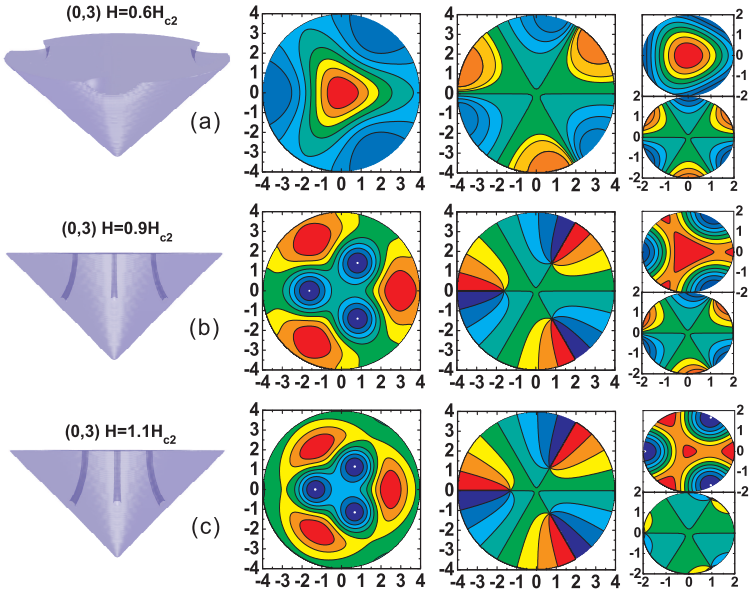

Fig. 4.10 The plots of the vortex configuration, Cooper-pair density and the phase of order parameter of the multivortex state (0,3) at the applied magnetic fields H/H_{c2}=0.6, 0.9, 1.1 for the circular cone (z_0=4ξ, θ=45°, r=4ξ). The Cooper-pair density and the phase of the order parameter are shown in the $z = 4\xi$ and $z = 2\xi$ planes.

From Fig. 4.8 and Fig. 4.9, we can find that at suitable applied magnetic field: (i) for the (0,L) L=2-6 states the number of vortices is L. They are located on a shell, while there is no vortex in the center. The vorticity is L. The highest Cooper-pair density is located at the apex of the circular cone; (ii) for the (1,L) L=4-6 states the number of vortices is L. (L-1) of them are located on a shell, while there is one vortex in the center along the z axis. The vorticity is L; (iii) for the (2,6) state the number of vortices is 5. Four of

them are located on a shell, while there is a giant vortex in the center along the z axis. The total vorticity is 6 while the giant vortex in the center has vorticity equal to 2; (iv) Notice also that the number of the vortices is not the same in all z-planes. Thus in the same sample we have regions with lower vorticity (they are for small z-values) and regions with higher vorticity (near the z=z_0 plane).

Next, we investigate the effects of changing the magnetic field. In Fig. 4.10, we show the vortex configuration, the plots of the order parameter and the order parameter in the z=4ξ and z=2ξ planes for the multivortex state (0,3) at different applied magnetic fields H/H_{c2}=0.6, 0.9, 1.2. The value of the iso-surface in the vortex configuration in Fig. 4.10(a) is 0.05, while the value of the others in Fig. 4.10 is 0.005. We find that in Fig. 4.10(a) there is no vortex in the circular cone. That is because the applied magnetic field is not sufficiently large to form vortices. With increasing applied magnetic field, the vortices of the multivortex state (0,3) will move in the direction of the center.

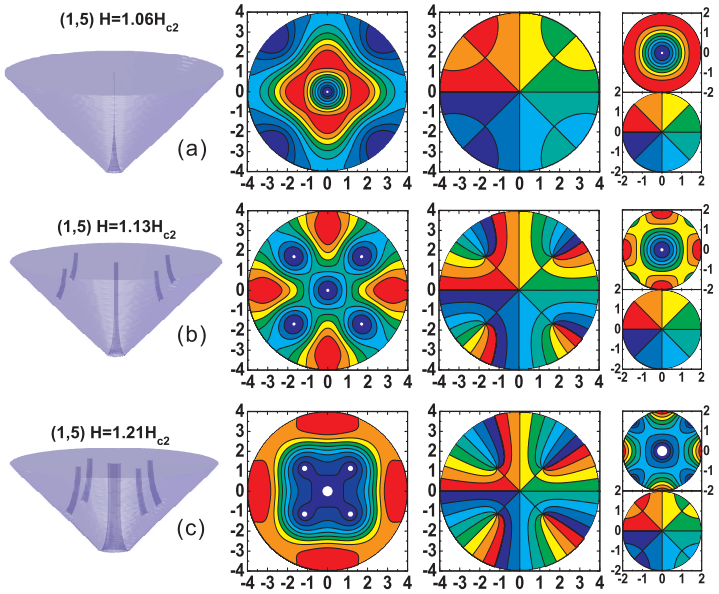

Fig. 4.11 The plots of the vortex configuration, Cooper-pair density and the phase of order parameter of the multivortex state (1,5) at the applied magnetic fields H/H_{c2}=1.06, 1.13, 1.21 for the circular cone (z_0=4ξ, θ=45°, r=4ξ). The Cooper-pair density and the phase of the order parameter are shown in the $z = 4\xi$ and $z = 2\xi$ planes.

To investigate the behavior of changing the applied field for the multivortex states (L_1, L_2), we show the same plots for the multivortex state (1,5) at

different applied magnetic fields H/H_{c2}=1.06, 1.13, 1.21 in Fig. 4.11. The values of iso-surface in the vortex configurations are different, for Fig. 4.11(a) it is 0.005, for the plot (b) it is 0.002, for the plot (c) it is 0.001. The small white holes in the plots of Cooper-pair density in Fig. 4.11 mean that the Cooper-pair density there is smaller than 0.001, but still different from zero. Here we find that: (i) when the applied magnetic field is not sufficiently large, there are no vortices away from center and the vortex in the center is very small; (ii) with increasing magnetic field, vortices around the center appear, they will move towards the center and become bigger.

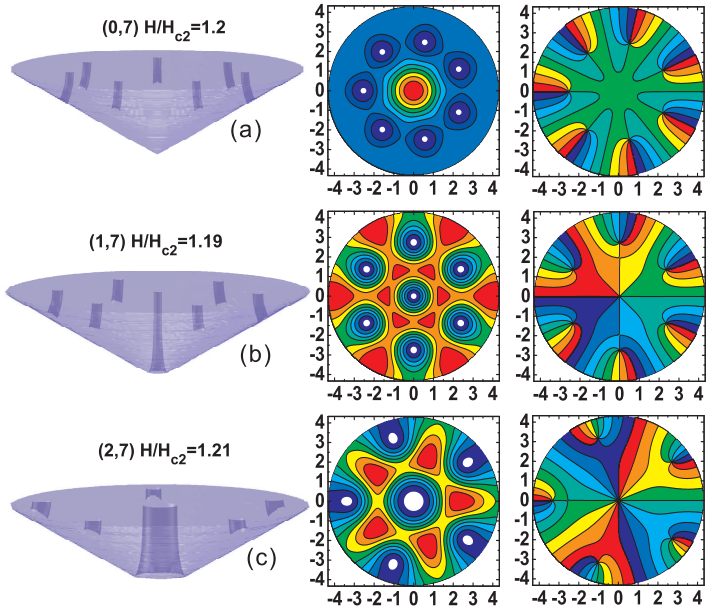

Fig. 4.12 The plots of the vortex configuration, Cooper-pair density and the phase of order parameter of the (meta-)stable multivortex states (0,7), (1,7) and (2,7) at the applied magnetic fields H/H_{c2}=1.2, 1.19, 1.21 for the circular cone (z_0=2.5ξ, θ=60°, $r \approx 4.33\xi$). The Cooper-pair density and the phase of the order parameter are shown in the $z = 4\xi$ plane. The white hole stands for the region where the Cooper-pair density is lower than 5×10^{-4}. The value of the iso-surface in the plots of vortex configuration is also equal to 5×10^{-4}.

Finally, we show the structure of the Cooper-pair density and the phase of the corresponding order parameter for the (meta-)stable multivortex states: (0,7) H/H_{c2}=1.2, (1,7) H/H_{c2}=1.19, (2,7) H/H_{c2}=1.21 in the circular cone (z_0=2.5ξ, θ=600, $r \approx 4.33\xi$) in Fig. 4.12. The white hole stands for the region where the Cooper-pair density is lower than 5×10^{-4}. The value of the

iso-surface in the plots of the vortex configuration is also equal to 5×10^{-4}. From Fig. 4.12 we also find that: for the multivortex state (0,7) at the applied magnetic field H/H_{c2}=1.2, there are seven vortices around the center, each of them has a vorticity equal to 1; for the multivortex state (1,7) at the applied magnetic field H/H_{c2}=1.19, there are six vortices around the center and one vortex along the axis. Each of them has a vorticity equal to 1; for the multivortex state (2,7) at the applied magnetic field H/H_{c2}=1.21, there are five vortices with vorticity equal to 1 around the center and one giant vortex with vorticity equal to 2 along the axis. These structures satisfy the discussion which we made before.

5

Conclusion

By making use of the linearized Ginzburg-Landau equation (LGL), we studied the superconducting states of a microscopic circular cone surrounded by vacuum with an external uniform magnetic field along its axis. As an approximation, the order parameter of a superconducting state is recognized as a linear combination of the eigenfunctions of the LGL equation. The coefficients of the linear combination are determined by minimizing the Gibbs free energy with respect to these coefficients and their complex conjugates. To obtain analytic expressions for the coefficients and the analytic stability conditions, we only consider the cases of one component (corresponds to the giant vortex states) and two components (corresponds to the multivortex states).

For the giant vortex states we numerically obtained the eigenvalue and the eigenfunction of the LGL equation, the Gibbs free energy, the order parameter, the largest-vorticity distribution diagram, the Cooper-pair density. We found that with increasing size of the circular cones the largest allowed vorticity increases (see Fig. 3.1). In case of larger vorticity, a circular cone has a narrower magnetic field region over which the giant vortex states are stable (see Fig. 3.3 and Fig. 4.7). With increasing applied magnetic field, the Cooper-pair density of a certain giant vortex state is suppressed (see Fig. 3.5). The giant vortex state with vorticity equal to zero does not have a vortex, the others have a giant vortex with a vorticity equal to its angular momentum quantum number. The vortex enters and exits the sample perpendicular to the surface of the circular cone (see Fig. 3.5). We showed that the excited giant vortex state (L=0, n=1) exists in a circular cone when the applied magnetic field is sufficiently low.

For the multivortex states (we limited ourselves to two components in the expression of the order parameter), we obtained the Gibbs free energy, the ground state, the Cooper-pair density (the vortex configuration) and the phase of the order parameter. There are also some (meta-)stable giant vortex states but sometimes with a narrower magnetic field region than that for the case we included only one component (see Fig. 4.1). Not all the combining multivortex states are (meta-)stable. It depends on the stability condition. A circular cone with a larger largest allowed vorticity has a more complex free energy vs. magnetic field diagram (see Fig. 4.1 and Fig. 4.3). For the states (L_1, L_2) where $L_2 > L_1$ at a sufficiently large applied magnetic field L_2-L_1 vortices are located around the axis, while there is one vortex with vorticity equal to L_1 in the center. Each vortex located around the center has a vorticity equal to one (see Fig. 4.8 and Fig. 4.9). When the applied magnetic field is not large enough, there will be no vortices existing around the center (see Fig. 4.10). With increasing applied magnetic field, vortices around the center will appear and move towards the center (see Fig. 4.11). All of the vortices enter and exit the circular cone perpendicular to the surface of the circular cone. Usually the ground state which has the lowest Gibbs free energy is mixed by the giant vortex states and the multivortex states (see Fig. 4.6 and Fig. 4.7).

To my knowledge this is the first study of the vortex states in a superconducting circular cone. In a preview related work (Ref. [14]), only the Meissner state of such a type of system was studied. In the present work we did not take into account the second Ginzburg-Landau equation and therefore the present analysis is valid for supercondectors with high κ-values.

References

1. S. V. Yampolskii and F. M.Peeters, Phys. Rev. B **62**, 9663 (2000).
2. V. A. Schweigert and F. M. Peeters, Phys. Rev. Lett. **83**, 2409 (1999).
3. R. Benoist and W. Zwerger, Z. Phys. B **103**, 377 (1997).
4. J. J. Palacios, Phys. Rev. B **58**, R5948 (1998).
5. P. Singha Deo, V. A. Schweigert, F. M. Peeters, and A. K. Geim, Phys. Rev. Lett. **79**, 4653 (1997).
6. V. A. Schweigert and F. M. Peeters, Phys. Rev. B **57**, 13817 (1998).
7. A. Kanda, B. J. Baelus, F. M. Peeters, K. Kadowaki and Y. Ootuka, Phys. Rev. Lett. **93**, 257002 (2004).
8. B. J. Baelus, S.V. Yampolskii and F. M. Peeters, Phys. Rev. B **65**, 024510 (2001)
9. Antonio R, de C. Romaguera, Mauro M. Doria and F. M. Peeters, Phys. Rev. B **75**, 184525 (2007).
10. B. J. Baelus, S. V. Yampolskii and F. M. Peeters, Phys. Rev. B **66**, 024517 (2002).
11. B. J. Baelus, D. Sun and F. M. Peeters, Phys. Rev. B **75**, 174523 (2007).

12. D. Sun, *Vortex structure in a Mesoscopic Superconducting Sphere* (Master.D thesis, 2006).

13. M. Poza, E. Bascones, J. G. Rodrigo, N. Agraït, S Vieira, and F. Guinea, Phys. Rev. B **58**, 11173 (1998).

14. V. R. Misko, V. M. Fomin and J. T. Devreese , Phys. Rev. B **64**, 014517 (2001).

15. V. V. Schmidt, P. Müller, and A. V. Ustinov, *The Physics of Superconductors: Introduction to Fundamentals and Applications* (Springer-Verlag, Berlin Heidelberg, 1997).

16. V. A. Schweigert, F. M. Peeters, and P. S. Deo, Phys. Rev. Lett. **81**, 2783 (1998).

17. M. Tinkham, *Introduction to Superconductivity* (McGraw Hill, New York, 1975).

18. C. Kittel, *Introduction to Solid State Physics* (John Wiley and Sons, New York, 1996).

19. B. Baelus, *Vortex matter in Mesoscopic Superconductors* (PH.D thesis, 2002).

20. D. Daint-James and P. G. de Gennes, Phys. Letters **7**, 306 (1963)

21. Ketterson , *Superconductivity* (Cambridge University Press, Cambridge, 1996).

22. A. I. Buzdin, Phys. Rev. B **47**, 11416 (1993).

23. O. Buisson, P. Gandit, R. Rammel, Y. Y. Wang, and B. Pannetier, Phys. Lett. A **150**, 36 (1990).